DANMARKS OG GRØNLANDS GEOLOGISKE UNDERSØGELSE RAPPORT 1997/46

Faults and joints in chalk, Denmark: Rørdal Quarry in Aalborg Graben

Lena Thrane and Kim Zinck-Jørgensen

GEOLOGICAL SURVEY OF DENMARK AND GREENLAND
MINISTRY OF ENVIRONMENT AND ENERGY

GEUS

DANMARKS OG GRØNLANDS GEOLOGISKE UNDERSØGELSE RAPPORT 1997/46

Faults and joints in chalk, Denmark: Rørdal Quarry in Aalborg Graben

Lena Thrane and Kim Zinck-Jørgensen

GEOLOGICAL SURVEY OF DENMARK AND GREENLAND
MINISTRY OF ENVIRONMENT AND ENERGY

GEUS

Faults and joints in chalk, Denmark: Rørdal Quarry in Aalborg Graben

For a period of three years, one of the production walls of Rørdal Quarry situated near Aalborg, where Maastrichtian chalk is exploited for the cement industry, has been mapped at different scales in terms of its fracture pattern and characteristics. The wall was scraped off as chalk exploitation proceeded, continuously revealing new sections through the faulted and fractured chalk body. Quantitative data, such as orientation (strike/dip) of faults and fractures, fracture density information (line samples) and 2D map area (for lenght population analysis) have been sampled during the three years and are presented in this report.

The research is part of the JOULE III research project: Equivalent volume modelling of dual porosity dual permeability hydrocarbon reservoirs. The objective of the research is to develop techniques for optimising the production from fractured dual porosity, dual permeability hydrocarbon reservoirs. This research is a contribution to the geological fracture characterisation.

Chalk in northern Jylland

The Upper Cretaceous and Danian of the Danish area are dominated by very pure, largely biogenic limestones. In the Early Maastrichtian global high stand all of the danish territory was transgressed as the culmination of the period of 35 mill. years (Cenomanian- Maastrichtian) during which the chalk was deposited in a shallow seaway running from the Cretaceous Atlantic in the west to Poland in the east, bordered by the Fennoscandian Precambrian Shield and the Middle Europe islands (fig. 1; Håkansson et al. 1974). The near-shore areas were dominated by greensands and biocalcarenites passing into biomicrites or chalks towards the basin. In the earlier part of the Danian the marine accumulation was largely confined to the Danish Basin (Håkansson & Thomsen 1979) and the Central Graben in the present North Sea. Chalks in northern Jylland are basinal and occupies regions with salt induced highs as well as fault controlled inversion structures - much like the situation in the Central Graben.

The Rørdal quarry is situated centrally in the Aalborg Graben, a prominent feature in the major northwest-southeast trending Sorgenfrei-Tornquist Fault Zone. This fault zone has been active at least since the Late Palaeozoic governed by a number of long-lived, typically NW-SE striking major faults, which have gone through several episodes of deformation in both extensional and compressional regimes (Liboriussen et al. 1987). During the Late Cretaceous a series of troughs, including the Aalborg Graben, developed along the zone, accumulating more than two kilometres of chalk in the deepest part of the basin (fig. 2). In the latest Cretaceous and earliest Tertiary these troughs became inverted in a series of compressional pulses related to the Alpine Orogeny, reactivating the major faults along the zone. The chalk level now exposed is the result of up to 1000 metres of Neogene uplift and subsequent erosion (Japsen 1993).

Glacial influence is largely erosional in northern Jylland with only local internal deformation of the chalk sequence. The melting of the icesheet, however, has induced horizontal, largely bed paralleling deloading fractures of the near surface part of the chalk sequence.

Maastrichtian and Danian chalks and limestones are exposed in the sub-Quaternary surface in a zone across northern Jylland (fig. 3). Mostly the rocks are covered by glacial and postglacial deposits, but in a series of quarries and natural outcrops the chalks and limestones are readily accessible.

Main lithologies include a more or less continuous spectrum of biogenic carbonate sediments ranging between the two dominant end members, pelagic chalk and bryozoan limestone (Bromley 1979). The insoluble residue is low, suggesting a low influence of terrestrial material. The chalk is intensively bioturbated with distinct burrows indicating deposition in mainly oxic conditions (Ekdale and Bromley, 1984). Sedimentation rate has been fairly high during the Maastrichtian (Håkansson et al. 1974). As a result of low to moderate post-depositional burial most on-shore chalk has suffered surprisingly mild diagenesis and has retained a very high primary porosity.

Except for the low diagenetic levels, Maastrichtian and Danian chalks and limestones in northern Jylland are considered close analogs to the chalk reservoirs in the North Sea.

Rørdal quarry

The locality is an active quarry covering an area of more than two square kilometres and up to 60 metres deep with quarrying activity taking place at three different levels. The investigations for this study have been concentrated on the middle level where the active vertical quarried wall is approximately 15 metres high and more than 1100 metres long, trending approximately N-S. The quarry exposes a number of steeply dipping, somewhat curved normal faults (fig. 4).

The sequence exposed in the eastern quarry wall can be divided into two faultbounded sections. The middle part of the profile, from 250-850 m (fig. 4) is dominated by chalk without flint (only a few nodules) alternating with dm thick marly beds, whereas the northernmost and southernmost part of the profile is dominated by chalk with thin, but distinct flintbands and only thin marly horizons. The northern part can easily be correlated with the southernmost part of the profile by means of the flintbands, which act as marker horizons.

An E-W trending old quarry wall in the southern part of the quarry exposes a series of low open folds. The folds are made visible by a number of marl bands and illustrates that the chalk has experienced some weak compression.

Stratigraphy and lithology

The chalk sequence exposed in the quarry spans the Lower/Upper Maastrichtian boundary as indicated by Surlyk, 1970, 1984) with the presence of the *tennicostata-semiglobularis* Zone (Brachiopod Zone 7) and the *semiglobularis-humboldtii* Zone (Brachiopod Zone 8).

The Maastrichtian white chalk is fairly homogeneous, composed almost exclusively of the calcitic skeletons of microscopic pelagic organisms with subordinate amounts of benthic skeletons, and a non-carbonate content usually well below 2 % (Håkansson et al. 1974). However, in Rørdal a significant part of the middle Maastrichtian chalk sequence exposed is displaying a primary cyclic pattern with dm thick marly horizons, where the non-carbonate content is as high as 18 %. A series of flint bands and flint nodules of diagenetic origin are present in some levels providing usefull stratigraphic marker horizons.

Porosity and permeability have been determined from a number of one inch core plugs. The average porosity is 46 % (ranging between 42 - 50 %) and the average permeability is 7.9 mD (ranging between 4.7 - 14 mD).

Faults and joints in Rørdal quarry

All faults and major fracture zones exposed in the active quarry wall has been mapped in the field and from photomosaic and orientation (strike/dip) of a number of faults has been measured (fig. 4). The great majority of faults are steeply dipping (50 - 90° ; fig. 5a). The faults are distributed as a conjugate set with an orientation NW-SE to NNW-SSE largely paralleling the regional structural gain (fig. 5b). The maximum stress axis was vertical and the orientation of striations on many fault surfaces indicate that pure dip-slip displacements were dominant for this fault set. One notable exception from this general fault pattern is illustrated by a major, east-west striking reverse fault (at '700m' on fig. 4). The relationship between the reverse fault and the normal fault set is not yet clear, but the reverse fault may be associated with the gentle folds found in the southern wall of the quarry.

Apart from the major faults the chalk is intersected by numerous joints. The majority of joints are also steeply dipping (60 - 90° ; fig. 5a). The orientation distribution cluster in two distinct conjugate sets, with one set paralleling the orientation of the fault set, and whereas the other set is oriented almost perpendicular (NE-SW)to the first set (fig. 5b).

Horizontal and subhorizontal joints, dipping less than 20° are also present in the quarry but are not as numerous (fig. 5a). The relationship between the joints and the steep conjugate joint sets is not settled. In some cases the conjugate joints are clearly displaced by the horizontal joints whereas in other cases the interaction between the two types is less obvious. Glacigenic thrusting or simply deloading are the most likely origin of the horisontal joints, which means they are late in origin and less relevant for subsurface conditions.

Fault data

For a period of three years (1994-1996) the N-S trending production wall was studied. As the chalk exploitation proceeded, new sections through the chalk was revealed. For each year a series of photograps was taken for a photomosaic of the wall, and orientation (strike/dip) of the faults was obtained. The wall section based on first year observations is presented in fig. 4.

Fault data obtained the first year are named RDH1, second year is RDH2 and third year is RDH3.

Orientation of faults

Orientation of faults for each year has been plotted in stereographic projection (Wulff) as normals to fault planes (fig. 6a, 7a, 8a) and as contours (fig. 6b, 7b, 8b). Fault orientations are summerized from all three field campains (fig. 9). The majority of fault cluster in the NW-SE to NNW-SSE direction which is also evident from the rose frequency diagrams of strike, where each data set have been plotted (fig. 10a, 10b, 10c) and the total data set (fig. 10d). Dip direction plotted as rose frequency diagrams for each data set (fig. 11a, 11b, 11c) and for the total data set (fig. 11d). The dip direction of faults is almost equally much towards ENE and WSW. Dip and dip direction for the total number of faults are also plotted as histograms in fig 5 along with joint data.

Joint data

Sampling of joint data has followed two fundamentally different approaches: Line samples and length populations. Line samples of joint populations have been colleted along horisontal lines where the positon of every joint has been marked and supplemented with orientation (strike/dip) measurements. Length population data sets have been collected in one square meter test areas and these map areas have been supplemented with orientation (strike/dip) measurements of the joints intersecting the area. Data has been sampled during several field campains.

Line samples of joints

The spacing between joints is established from horizontal line samples on vertical quarry walls. As the majority of joints are steep to very steep with a dip of 60° or more the horizontal line sampling employed is considered to be at a sufficiently high angle to the overall fracture orientation. Length of horisontal lines vary from 5 to 30 metres. In addition to its position on the line the orientation (strike/dip) of each joint has been determined.

Four line samples have been collected (RD2, RD3, RD4 and RD5). RD1 only includes orientation (strike/dip) data.

Orientation of joints

The orientation of the joint in the line samples were measured as strike/dip and subsequently plottet in a Wulff projection as normals to fracture planes (figs. 12a, 13a, 14a, 15a, 16a,) and as contours (figs. 12b, 13b, 14b, 15b, 16b). The orientation of joints are somewhat scattered, however, with a tendency to cluster around a NNW-SSE direction and a ENE-WSW direction. The total number of orientation measurements of joints are plotted in Wulff projections (fig. 17) where the two dominating orientation direction becomes very clear and with NNW-SSE as the dominant orientation. Rose frequency diagrams of strike for each data set (figs. 18a, 18b, 18c, 18d, 18e) and for the total number of joints (fig. 18f) shows that the majority of joints are oriented parallel to the faults in the quarry.

Dip direction has been plotted as rose frequency diagrams for each data set (figs. 19a, 19b, 19c, 19d, 19e) and for the total number of joints (fig. 19f). Like the faults in the area the joints are dipping equally much towards ENE and WSW.

Dip and dipdirection for the total number of joints measured in the quarry have been plottet as histograms in fig. 5 along with fault data.

Spacing of joints in line samples

The length of the four horisontal line samples (RD2, RD3, RD4 and RD5) varies from 5 to 30 metres. The position of joints along each line was marked and the density of joints is presented in fracture logs (figs. 20, 21, 22, 23) where each measured fracture is marked by a vertical line.

The joints have been divided into two sets according to their orientation and density distribution of each set has been analysed individually and for each data set the coefficient of variation (CV) of the density has been calculated. For two of the line samples (RD2 and RD4) two data sets are analysed for each line sample, whereas for line sample RD3 and RD5 only one data set has been analysed for each line sample as the number of data belonging to the second orientation data set set was very limited. Density statistics are summerized in table 1.

TABLE 1

	Mean	SD	CV
RD2, data set 1	0.32	0.42	1.33
RD2, data set 2	0.26	0.22	0.89
RD3, data set 1	0.46	0.59	1.27
RD4, data set 1	0.17	0.11	0.64
RD4, data set 2	1.11	0.88	0.79
RD5, data set 1	0.48	0.27	0.58

Table 1: Mean, standard deviation (SD) and coefficient of variation (CV) of joint density for each subdirectional joint set.

The density data sets for each line sample are plotted as spacing/frequency histograms and as spacing/cummulative-number diagrams.

The histograms of the spacing distribution of the fracture sets (figs. 24a, 25a, 26a, 27a) show that the great majority of fractures within each subdirectional set are densily spaced.

CV values for the density data sets varies between 0.6 (anticlustering) and 1.3 (clustering) indicating that the density of fractures are approaching a random spacing (CV = 1 is random spacing) . The close approximation to a random spacing of fractures is further indicated by the spacing/cummulative-number diagrams (figs. 24a, 25a, 26a, 27a) where the density distribution of each fracture set is plotting close to straight lines when plotted on log-linear axes, indicating a negative exponential distribution for the datasets investigated.

Length populations

Length population data were collected from five 1 m^2 areas on the vertical quarry wall. The areas were selected to cover characteristic combinations of lithology and structural setting, including fairly homogeneous, pure chalk positioned far from major faults and in the immediate vicinity of a major fault, as well as the more marly chalk.

Three areas are presented in fig 28. Area **A** and **B** are from the sourthen end of the profile in the fairly homogeneous, pure chalk with flint bands; **A** is situated between major faults and **B** is situated in the immediate vicinity of a major fault but in similar lithology. Area **C** is situated in the rythmic marly chalk sequence far from major faults where the upper third of the area is within a marl band. The orientation of all areas are from left to right N-S.

Joint length for each area has been plottet as length/fequency histograms and as length/cummulative number diagrams (figs. 29, 30, 31). For each area the the coefficient of variation (CV) of the length distribution has been calculated (Table 2).

TABLE 2

	Mean	SD	CV
Rørdal A	0.19	0.17	0.90
Rørdal B	0.13	0.12	0.90
Rørdal C	0.17	0.18	1.04

Table 2: Mean, standard deviation (SD) and coefficient of variation (CV) of joint length for area A, B and C.

Cofficient of variation of length distribution for the three sets varies between 0.9 and 1.0 indicating a random distribution. The length distribution of each area is plotting close to straight lines when plotted on log-linear axes (fig. 29a, 30a, 31a), indicating a negative exponential distribution for the datasets investigated.

Two areas (**D** and **E**) are presented in fig. 32. Both areas are taken from the pure chalk sequence in the southern part of the profile, positioned at some distance to major faults. The orientation of sample area **D** is E-W (fig. 32a) and N-S for area **E** (fig. 32b). The orientation (strike) of joints are presented as rose frequency diagrams in fig 32c og 32d.

The orientation of the joint within each area were measured as strike/dip and subsequently plottet in a Wulff projections as normals to fracture planes (figs. 33a, 34a) and as contours (figs. 33b, 34b). The joint orientations are somewhat scattered, however, with a tendency to cluster around a NW-SE direction and a ENE-WSW direction in accordance with joint orientation in general from the quarry. The majority of joints are steeply dipping (70 - 90°) which also is accordance with the overall joint dip orientations in the quarry. Dip direction has been plotted as rose frequency diagrams for each area (figs. 35a and b).

The joints have been divided into two subdirectional sets according to their dip-direction and plottet in length/frequency histograms and as length/cummulative number diagrams (figs. 36, 37). For each directional subset in the two areas the coefficient of variation (CV) of length distribution has been calculated (Table 3).

TABLE 3

	Mean	SD	CV
Rørdal D, data set 1	0.30	0.21	0.69
Rørdal D, data set 2	0.19	0.15	0.79
Rørdal E, data set 1	0.48	0.28	0.59
Rørdal E, data set 2	0.37	0.16	0.43

Table 3: Mean, standard deviation (SD) and coefficient of variation (CV) for each subdirectional joint set.

Cofficient of variation of length distribution for four subdirectional sets varies from 0.4 to 0.9. The length distribution of each subdirectional set is plotting close to straight lines when plotted on log-linear axes (fig. 36a, 37a,)

Connectivity

The joint pattern found in the chalk can be characterized as a triangular pattern. The connectivity is considered to be high in general, as estimated from the joint patterns in the 1 m^2 areas. This estimate is based on the high number of connected joints with only a few dead ends present in all areas. It should be pointed out that the evaluation of connectivity is based strictly on geometrical evaluation of the joint patterns, whereas the actual connectivity at joint junctions has not been assessed in the field.

References

Håkansson, E., Bromley, R. & Perch-Nielsen, K. 1974: Maastrichtian chalk of north-west Europe - a pelagic shelf sediment. Spec. Publs. int. Ass. Sediment. **1**, 211-233.

Håkansson, E. & Surlyk, F. (in press): Geology of Denmark. In: Moores, E.M. & Fairbridge, R.W. (Eds): Encyclopedia on World Regional Geology. Chapman & Hall.

Japsen, P. 1993: Influence of lithology and Neogene uplift on seismic velocities in Denmark: Implications for depth consersion of maps. AAPG Bull. V. 77, No. 2, 194-211.

Liboriussen, J., Ashton, P. & Tygesen, T. 1987: The tectonic evolution of the Fennoscandian Border Zone In Denmark. Tectonophysics, **137**, 21-29.

Surlyk, F. 1970: Die stratigraphie des Maastricht von Dänemark und Norddeutschland aufgrund von Brachiopoden. News. Stratigr., 1, 7-16.

Surlyk, F. 1984: The Maastrichtian Stage in NW-Europe and its brachiopod zonation. Bull. geol. Soc. Denmark, 33 (1/2): 217-224.

List of figures

Figure 13: Stereographic projection (Wulff, lower hemisphere) of joint orientations in Rørdal Quarry (RD2). a) normals to fault planes, b) contour plot. Number of measurements is 84.

Figure 14: Stereographic projection (Wulff, lower hemisphere) of joint orientations in Rørdal Quarry (RD3). a) normals to fault planes, b) contour plot. Number of measurements is 28.

Figure 15: Stereographic projection (Wulff, lower hemisphere) of joint orientations in Rørdal Quarry (RD4). a) normals to fault planes, b) contour plot. Number of measurements is 67.

Figure 16: Stereographic projection (Wulff, lower hemisphere) of joint orientations in Rørdal Quarry (RD5). a) normals to fault planes, b) contour plot. Number of measurements is 13.

Figure 17: Stereographic projection (Wulff, lower hemisphere) of joint orientations in Rørdal Quarry (RD1 + RD2 + RD3 + RD4 + RD5). a) normals to fault planes, b) contour plot. Number of measurements is 215.

Figure 18: Rose frequency diagrams of joint orientations (strike) from Rørdal Quarry.

Figure 19: Rose frequency diagrams of joint orientations (dip direction) from Rørdal Quarry.

Figure 20: Horisontal line sample profile (RD2) from Rørdal Quarry. Joints are marked by vertical lines.

Figure 21: Horisontal line sample profile (RD3) from Rørdal Quarry. Joints are marked by vertical lines.

Figure 22: Horisontal line sample profile (RD4) from Rørdal Quarry. Joints are marked by vertical lines.

Figure 23: Horisontal line sample profile (RD5) from Rørdal Quarry. Joints are marked by vertical lines.

Figure 24: Density distribution of joints in RD2 line sample profile, Rørdal Quarry. Joints have been divided into two sets based on their orientation. a) Spacing versus cummulative number showing almost straight lines for both fracture sets on a log-linear plot. b) histogram of spacing versus frequency for the two fracture sets.

Figure 25: Density distribution of joints in RD3 line sample profile, Rørdal Quarry. Joints have been divided into two sets based on their orientation, only one set is plotted as number of data in the second set was too limited. a) Spacing versus cummulative number showing almost straight lines for both fracture sets on a log-linear plot. b) histogram of spacing versus frequency for the two fracture sets.

Figure 26: Density distribution of joints in RD4 line sample profile, Rørdal Quarry. Joints have been divided into two sets based on their orientation. a) Spacing versus cummulative number showing almost straight lines for both fracture sets on a log-linear plot. b) histogram of spacing versus frequency for the two fracture sets.

Figure 27: Density distribution of joints in RD5 line sample profile, Rørdal Quarry. Joints have been divided into two sets based on their orientation, only one set is plotted as number of data in the second set was too limited. a) Spacing versus cummulative number showing almost straight lines for both fracture sets on a log-linear plot. b) histogram of spacing versus frequency for the two fracture sets.

Figure 28: Joint pattern in three vertical sections each covering one square meter. a) joint pattern in fairly homogeneous, pure chalk between major faults. b) joint pattern in fairly homigeneous, pure chalk close to major fault. c) joint pattern in marly chalk sequence, upper third of the section is a marl band.

Figure 29: Joint length distribution in area A. a) plot of joint length versus cummulative number. b) joint length versus frequency.

Figure 30: Joint length distribution in area B. a) plot of joint length versus cummulative number. b) joint length versus frequency.

Figure 31: Joint length distribution in area C. a) plot of joint length versus cummulative number. b) joint length versus frequency.

Figure 32: a) and b): joint pattern in two vertical sections each covering one square meter, both are from fairly homogeneous, pure chalk between major faults. c) and d): rowe frequency diagrams of joint orientation (strike) in each area.

Figure 33: Stereographic projection (Wulff, lower hemisphere) of joint orientations in area D, Rørdal Quarry. a) normals to fault planes, b) contour plot. Number of measurements is 18.

Figure 34: Stereographic projection (Wulff, lower hemisphere) of joint orientations in area E, Rørdal Quarry. a) normals to fault planes, b) contour plot. Number of measurements is 35.

Figure 35: Rose frequency diagrams of joint orientations (dip direction) from Rørdal Quarry. a) area D, b) area E.

Figure 36: Joint length distribution in area D. Joints have been divided into two sets based on their orientation. a) plot of joint length versus cummulative number. b) joint length versus frequency.

Figure 37: Joint length distribution in area E. Joints have been divided into two sets based on their orientation. a) plot of joint length versus cummulative number. b) joint length versus frequency.

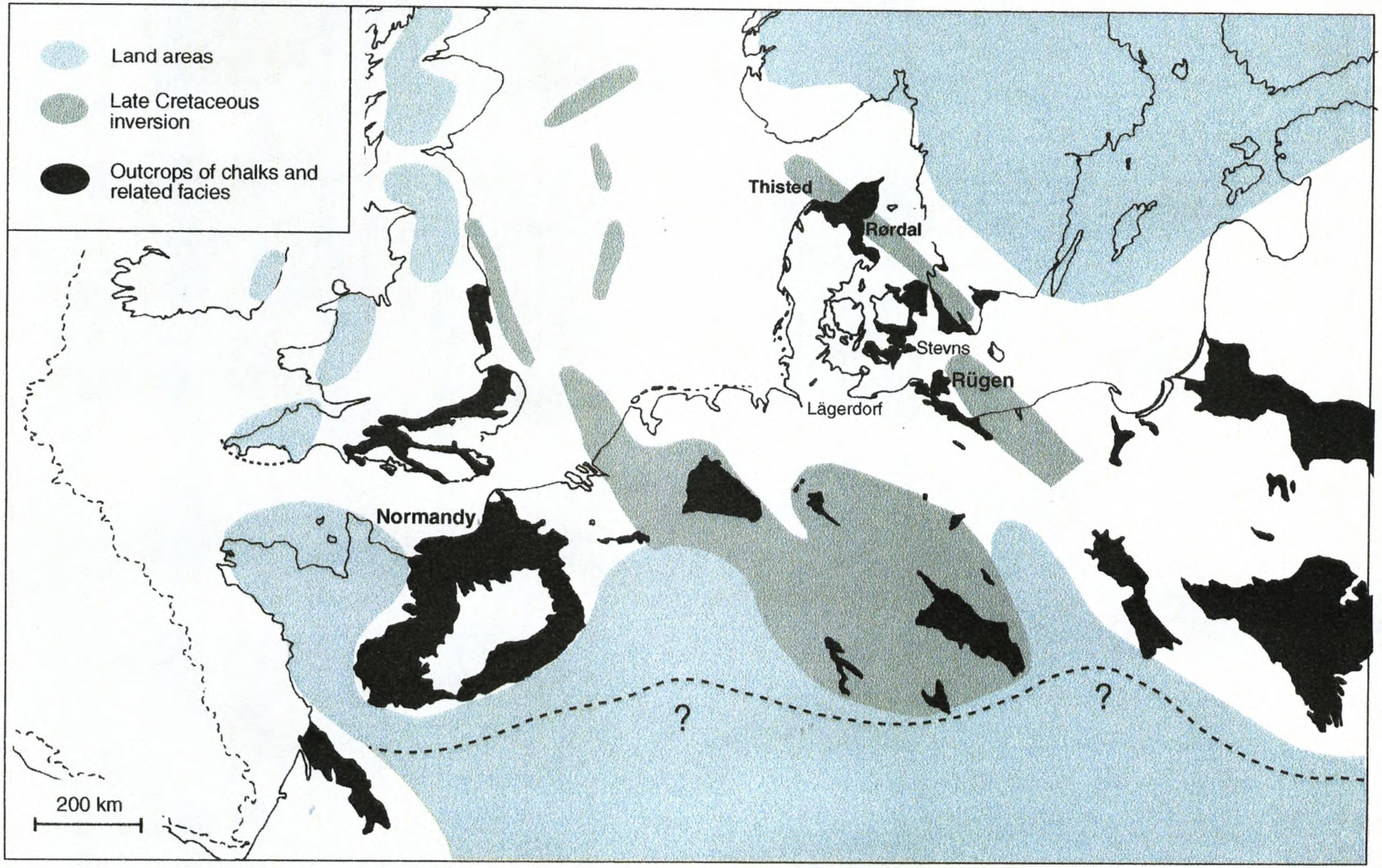
Land areas
Late Cretaceous inversion
Outcrops of chalks and related facies
Thisted
Rørdal
Stevns
Rügen
Lägerdorf
Normandy
?
?
200 km
Figure 1

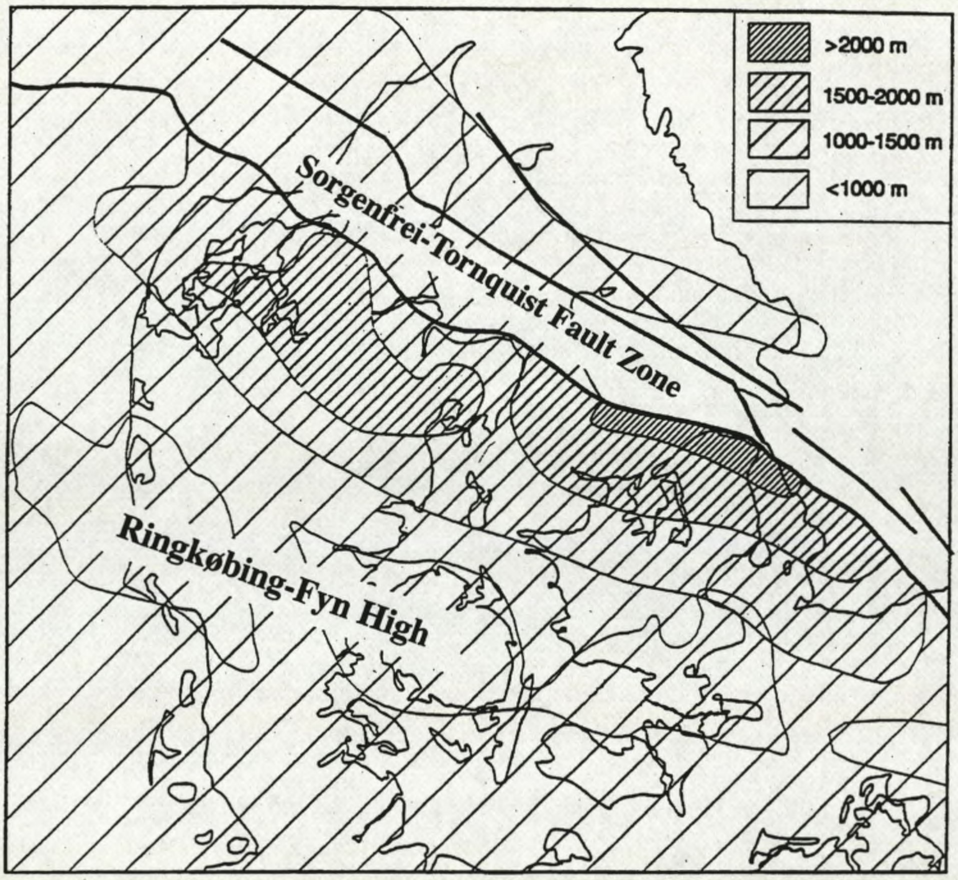
>2000 m
1500-2000 m
1000-1500 m
<1000 m
Sorgenfrei-Tornquist Fault Zone
Ringkøbing-Fyn High

Fig. 2

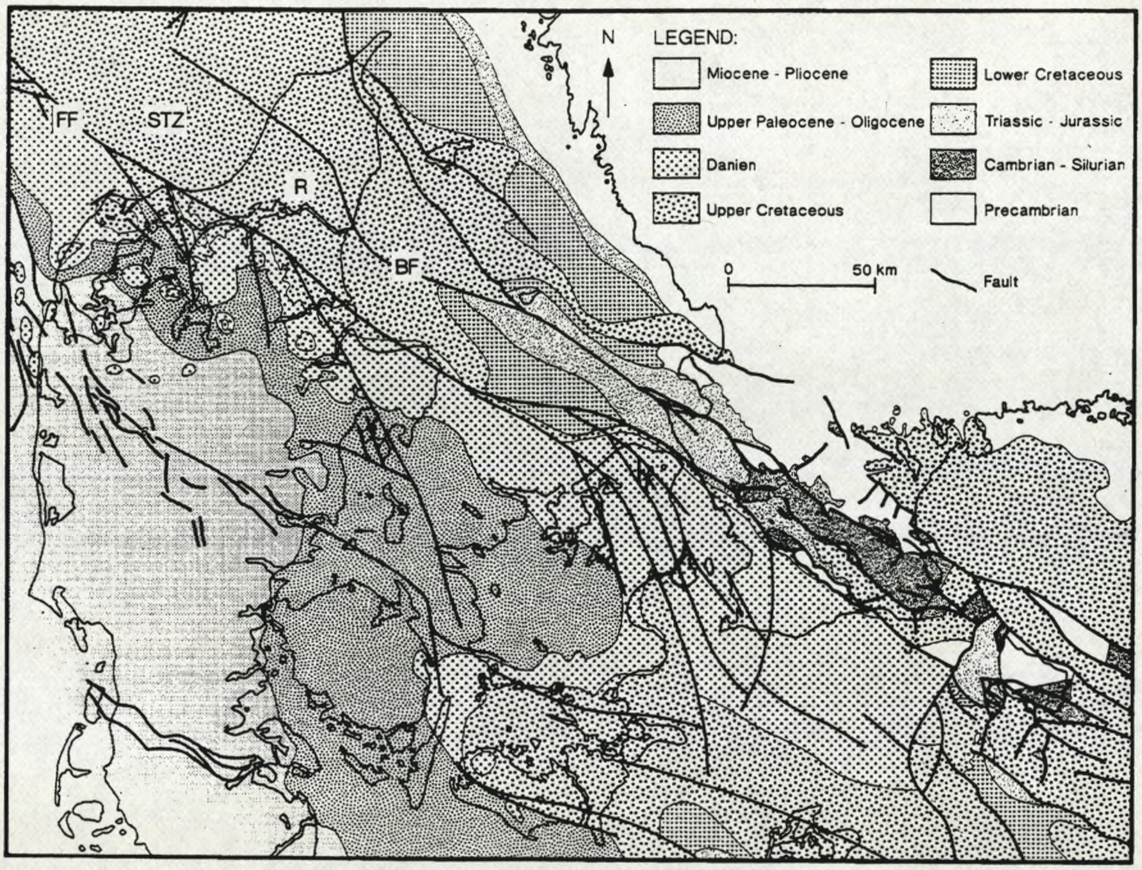

N
LEGEND:
Miocene - Pliocene
Upper Paleocene - Oligocene
Danien
Upper Cretaceous
Lower Cretaceous
Triassic - Jurassic
Cambrian - Silurian
Precambrian
0
50 km
Fault
FF
STZ
R
BF

Fig. 3

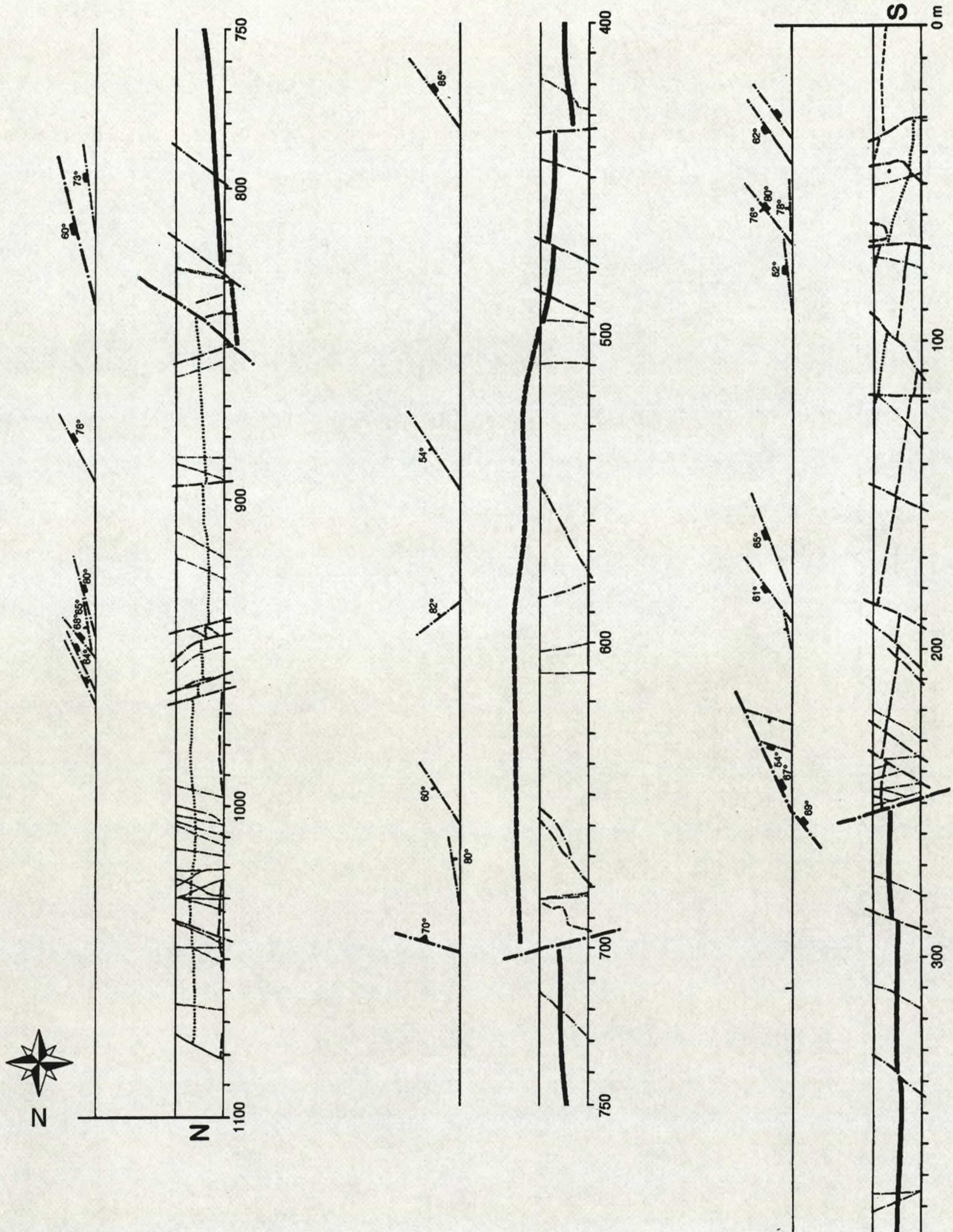

Fig. 4

Rørdal

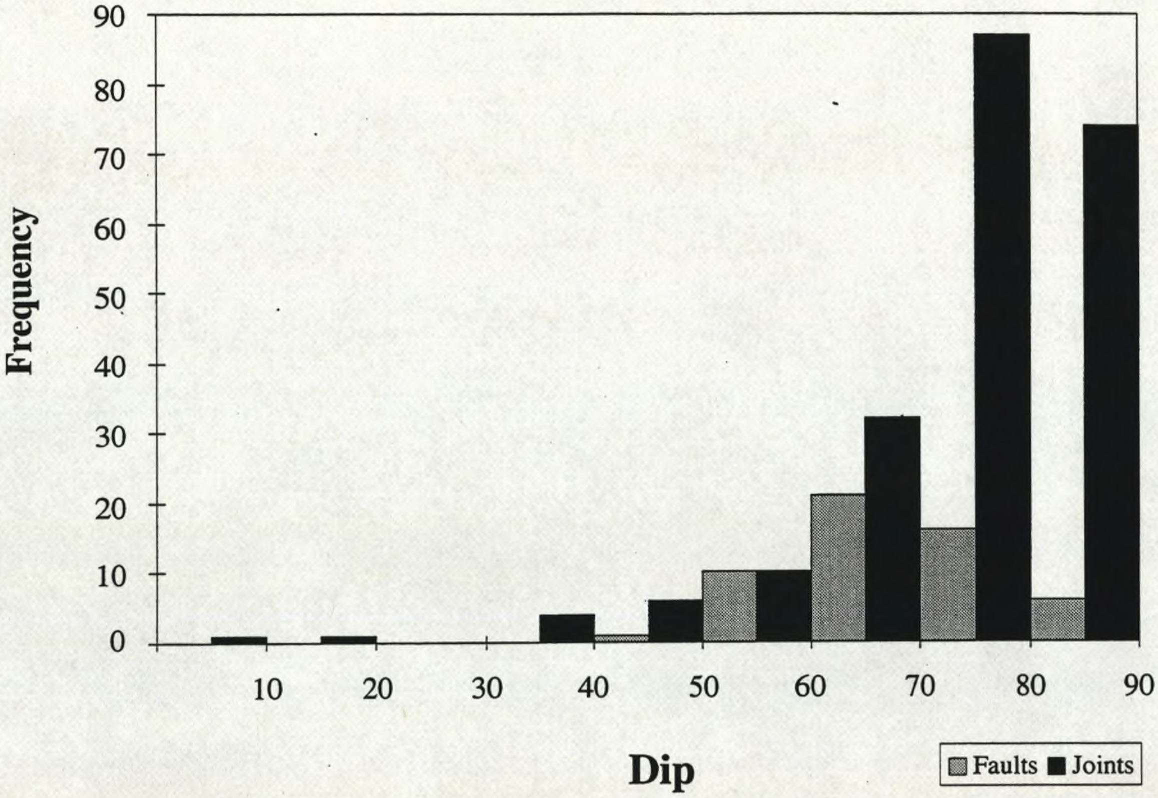

a

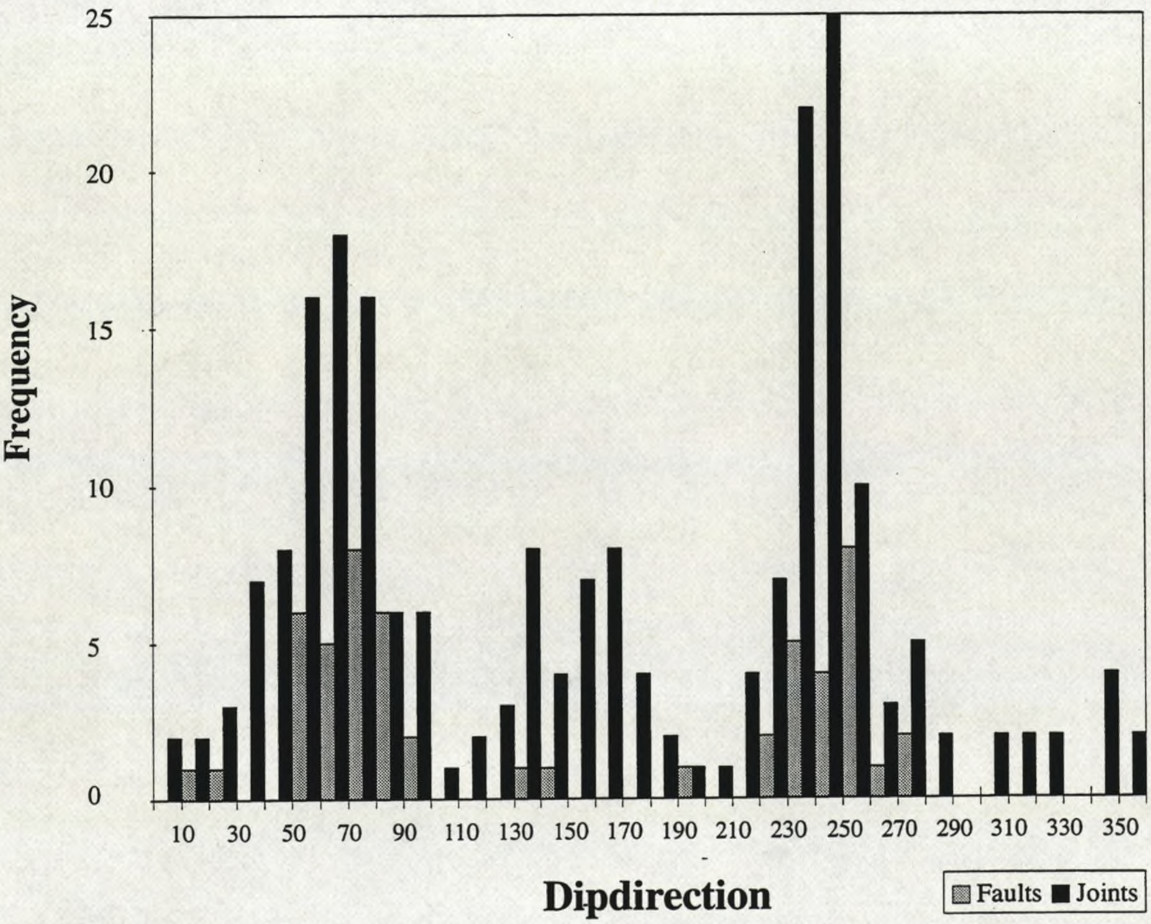

b

Fig. 5

RØRDAL-RDH1

Wulff projection

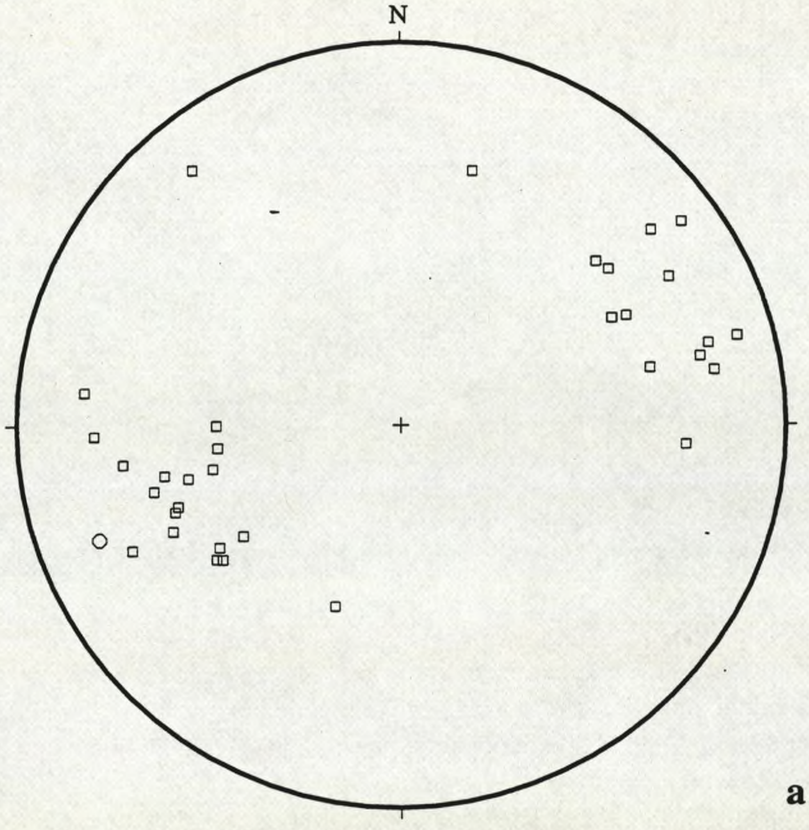

a

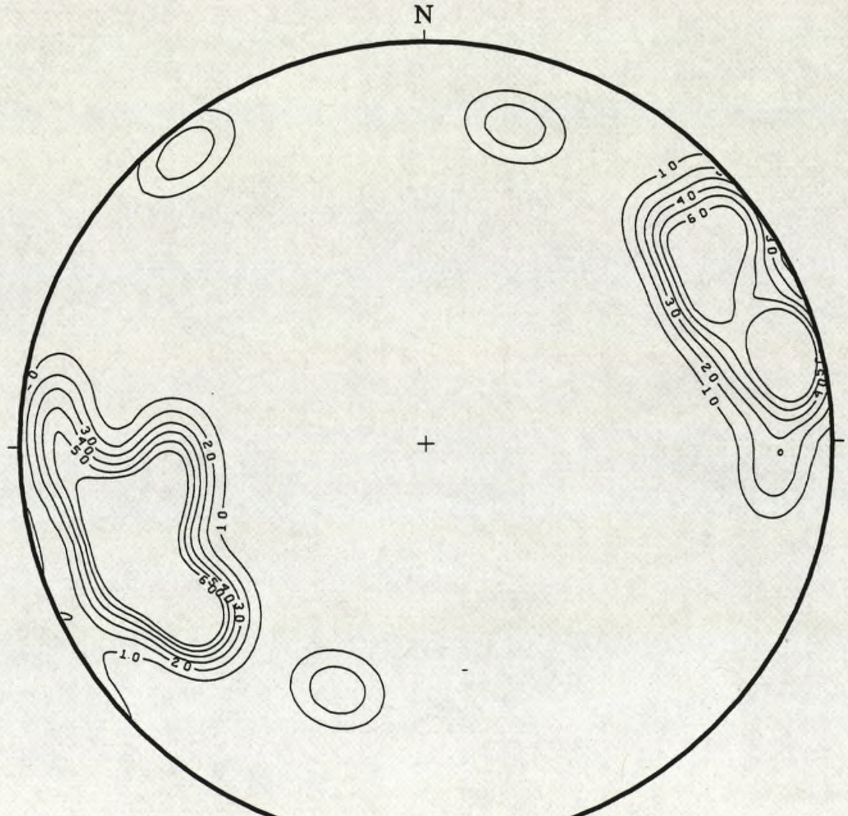

b

Fig. 6

RØRDAL-RDH2

Wulff projection

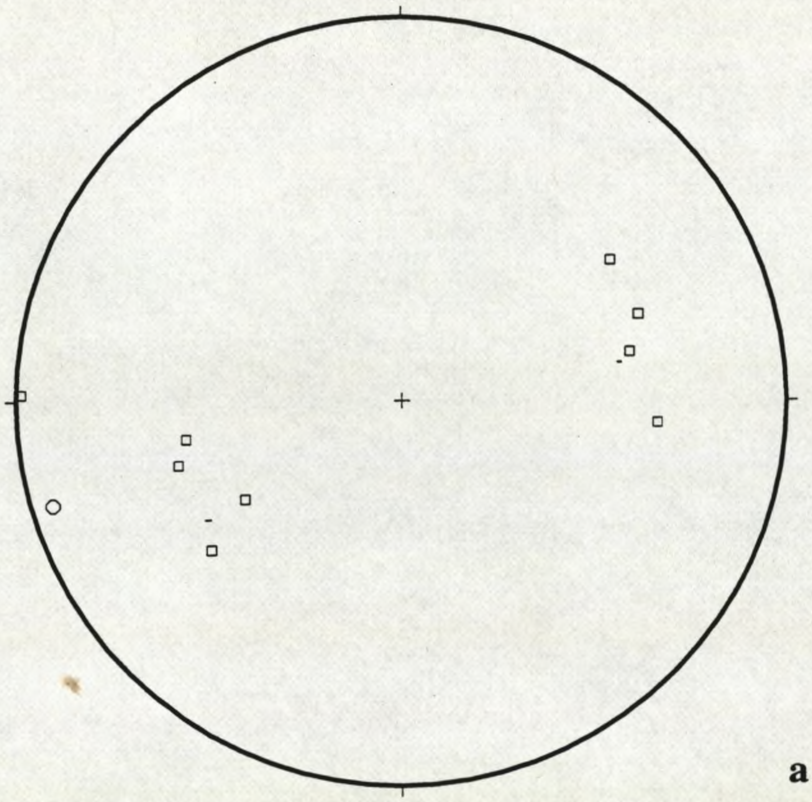

a

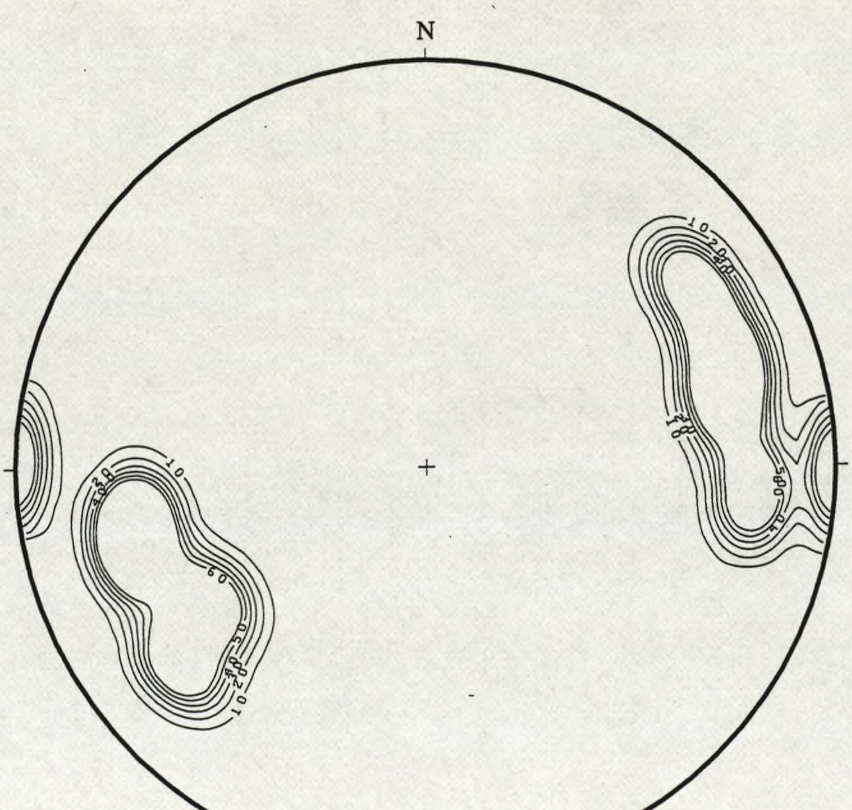

b

Fig.7

RØRDAL-RDH3

Wulff projection

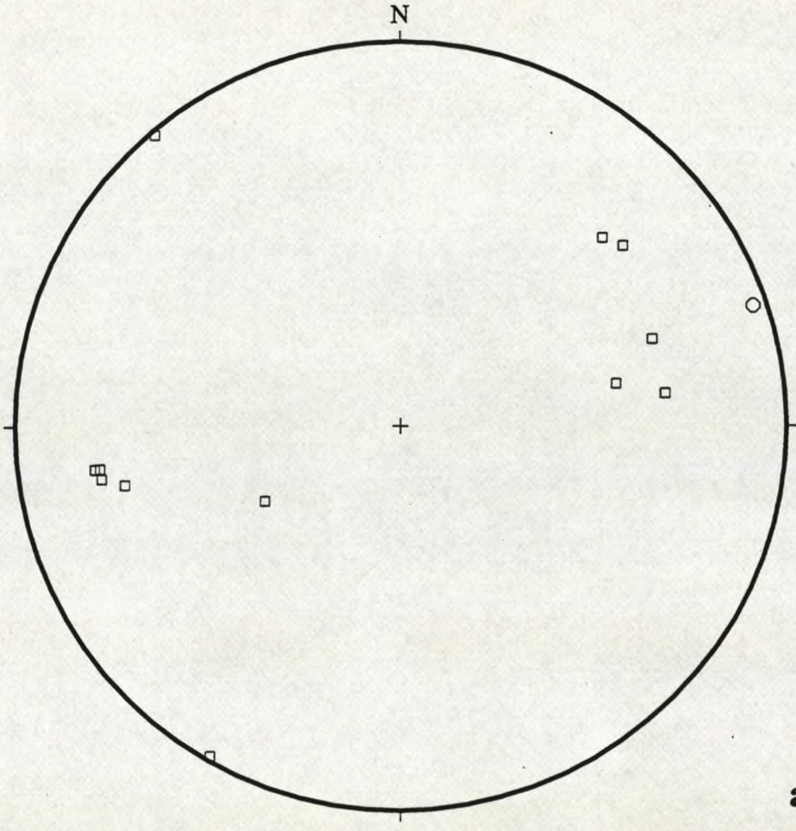

a

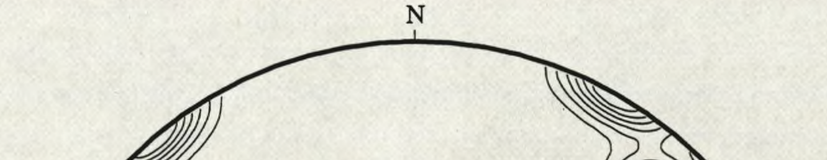

b

Fig. 8

RØRDAL-RDH1,RDH2,RDH3

Wulff projection

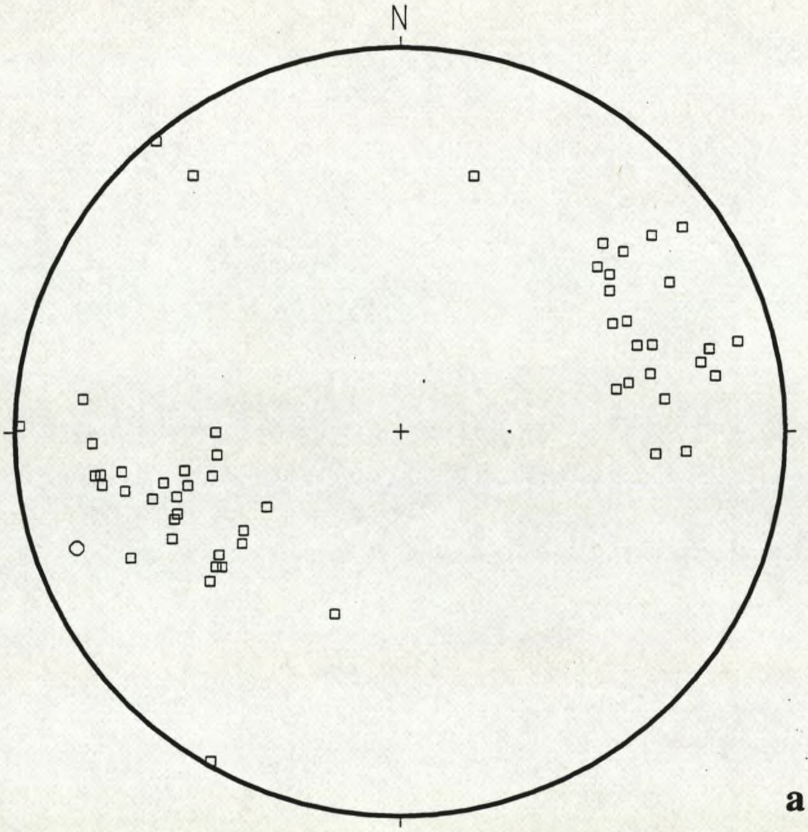

a

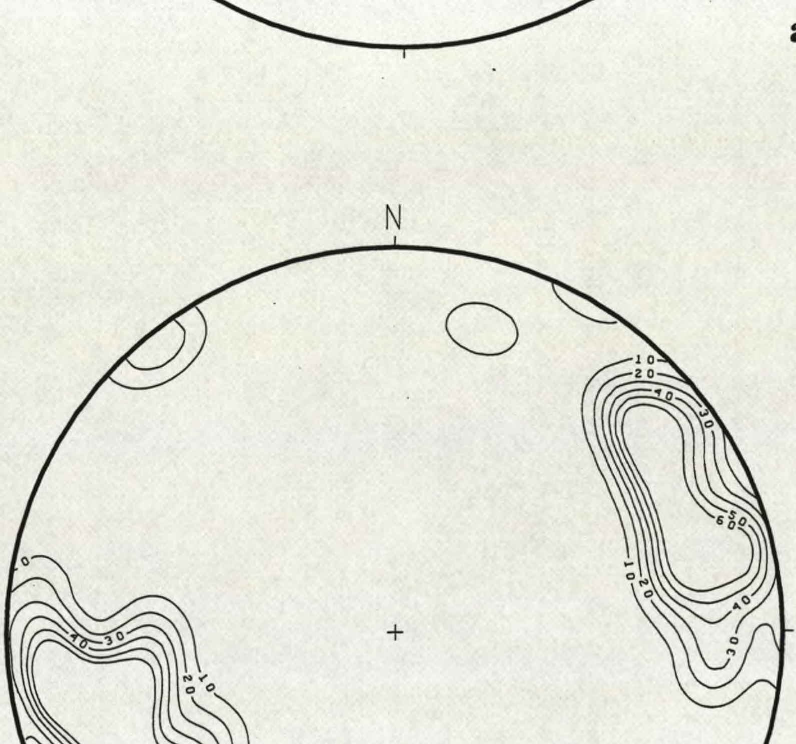

b

Fig. 9

Rørdal strike

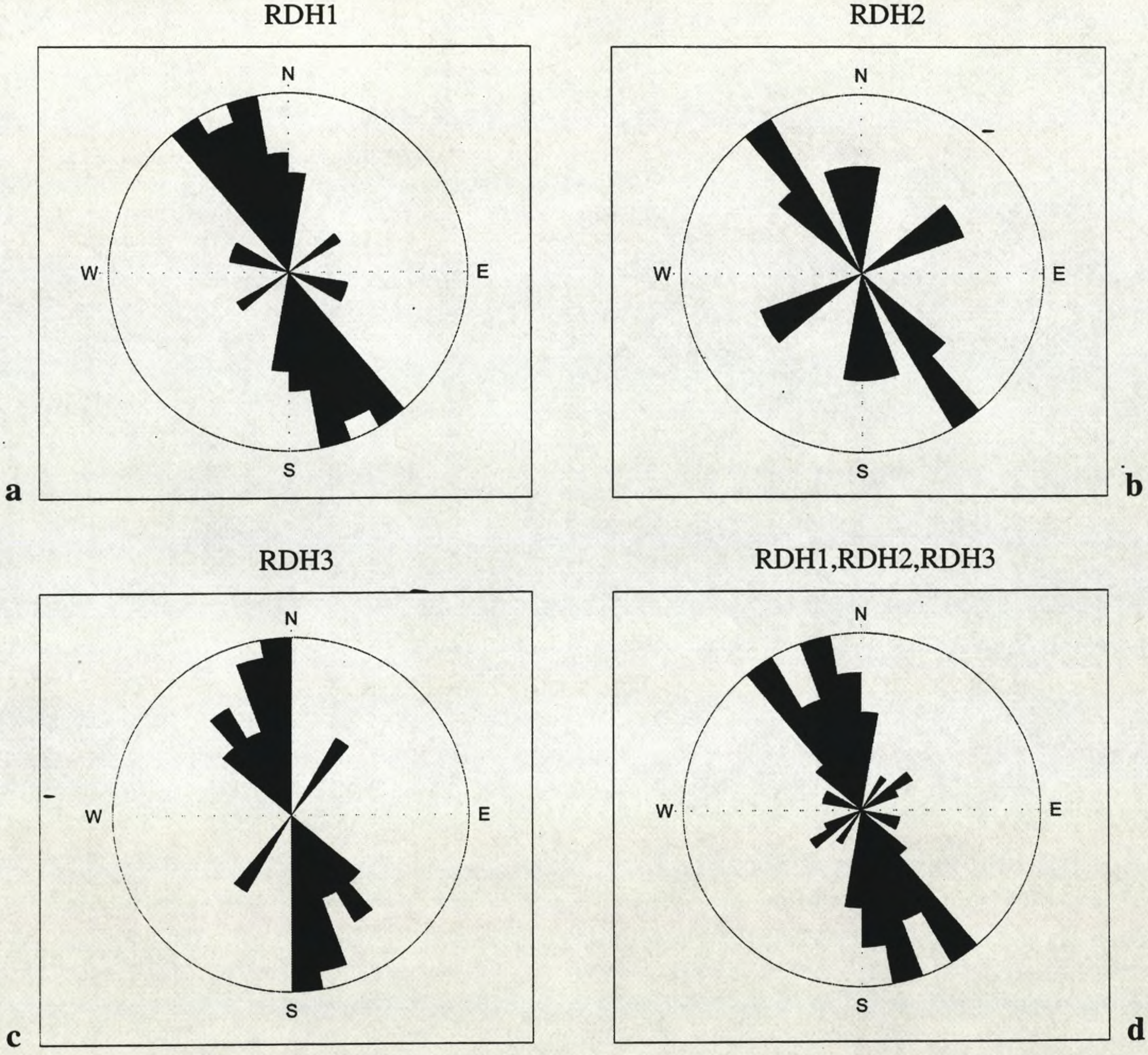

Fig. 10

Rørdal dipdirection

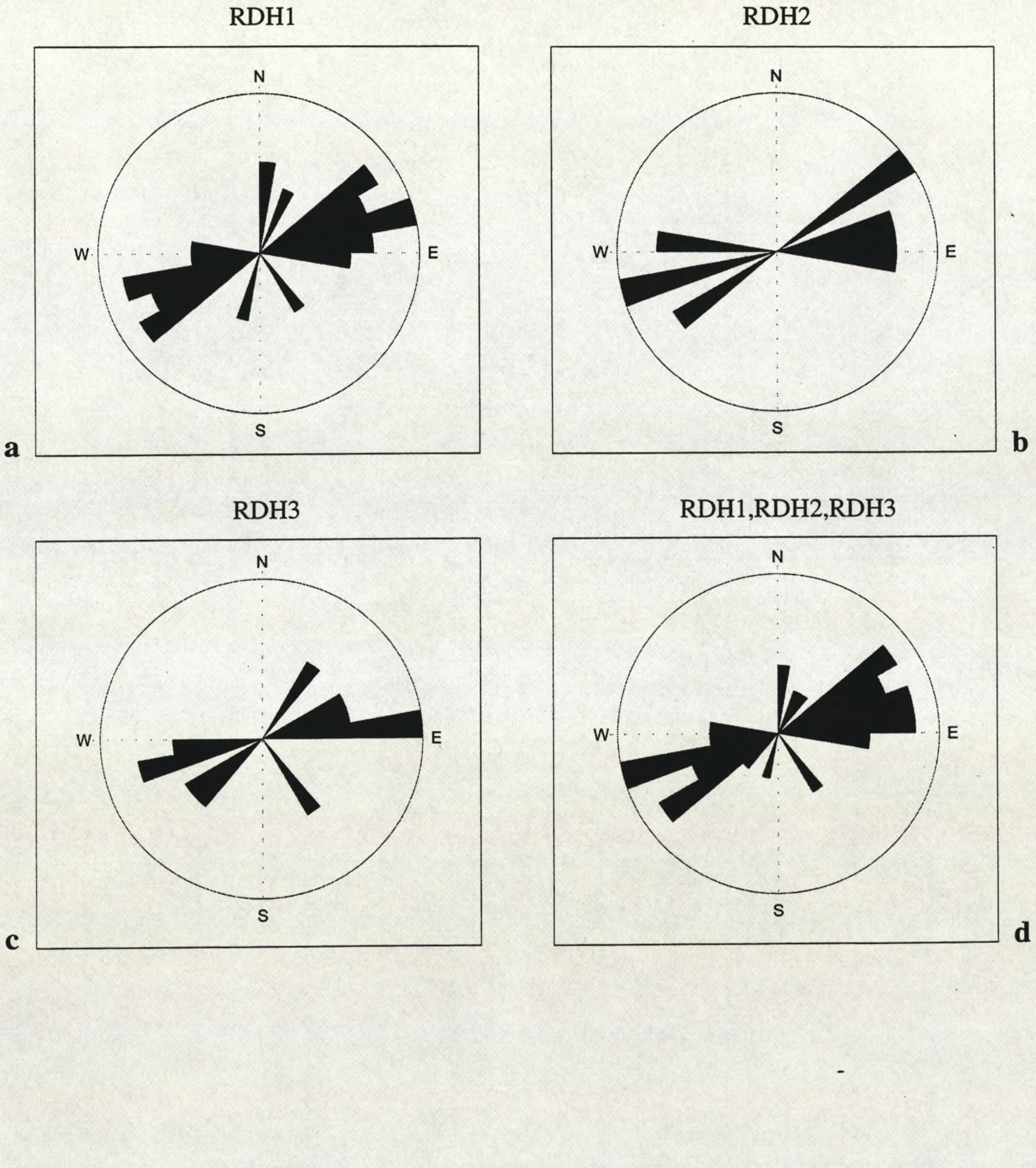

Fig. 11

RØRDAL-RD1

Wulff projection

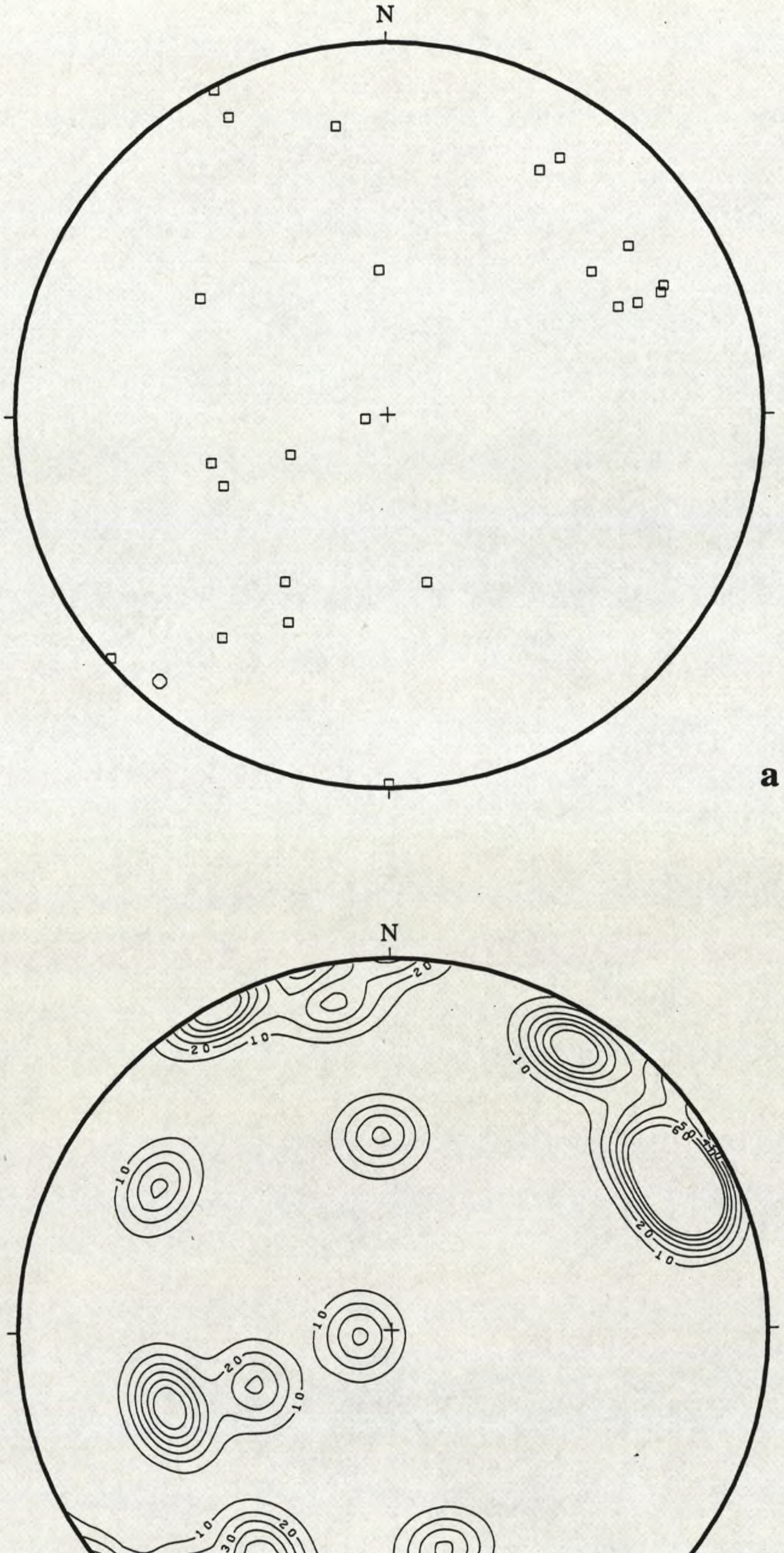

Fig. 12

RØRDAL-RD2

Wulff projection

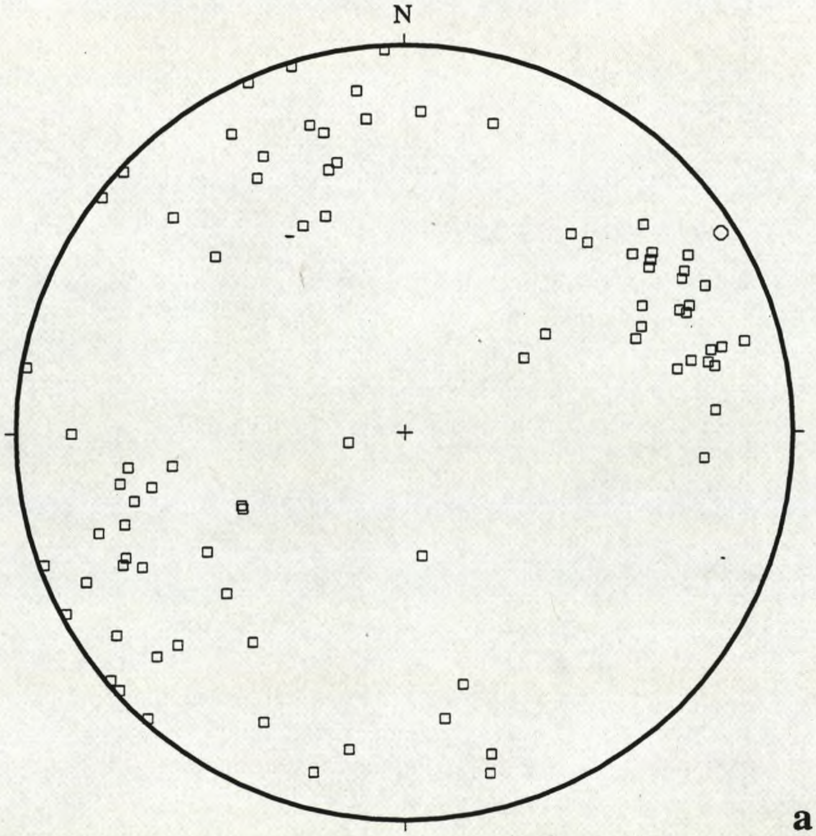

a

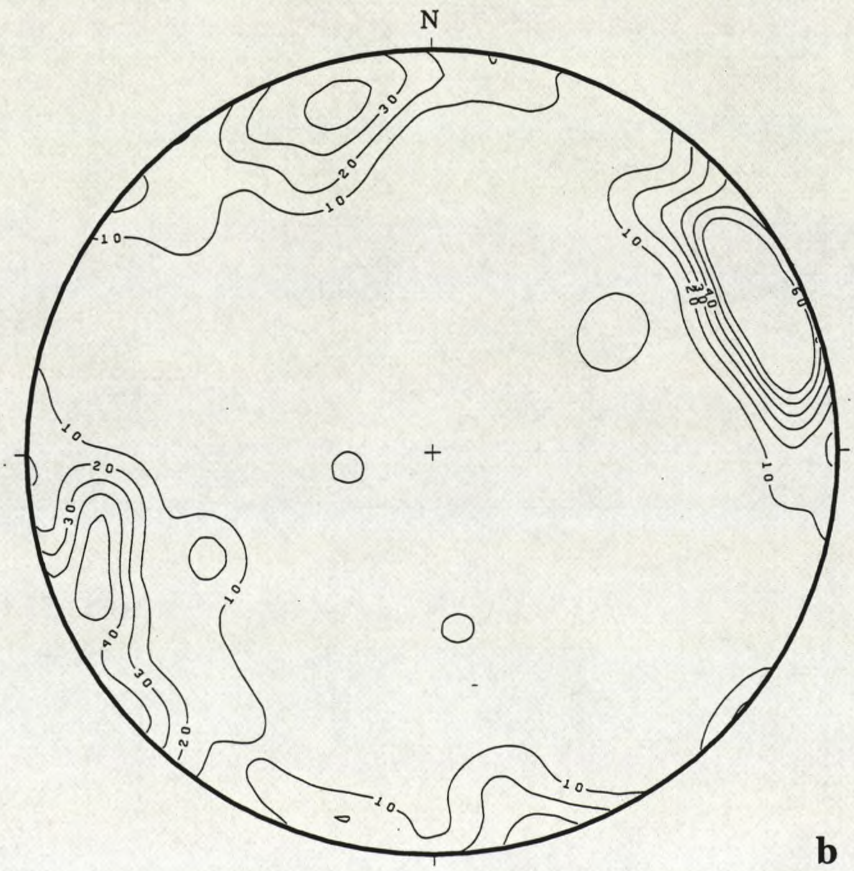

b

Fig. 13

RØRDAL-RD3

Wulff projection

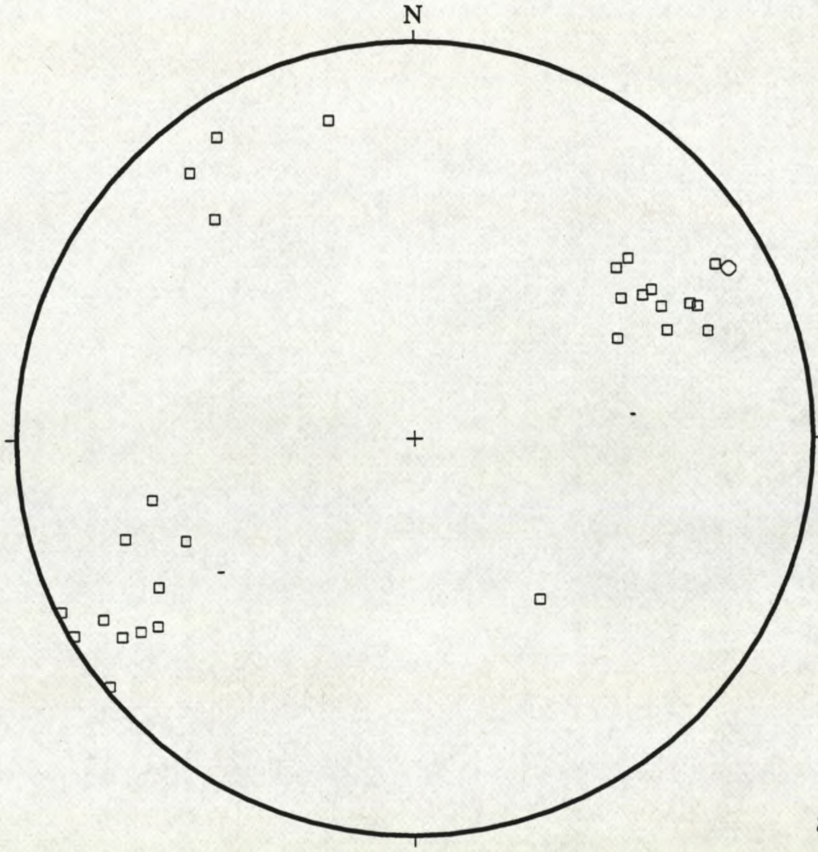

a

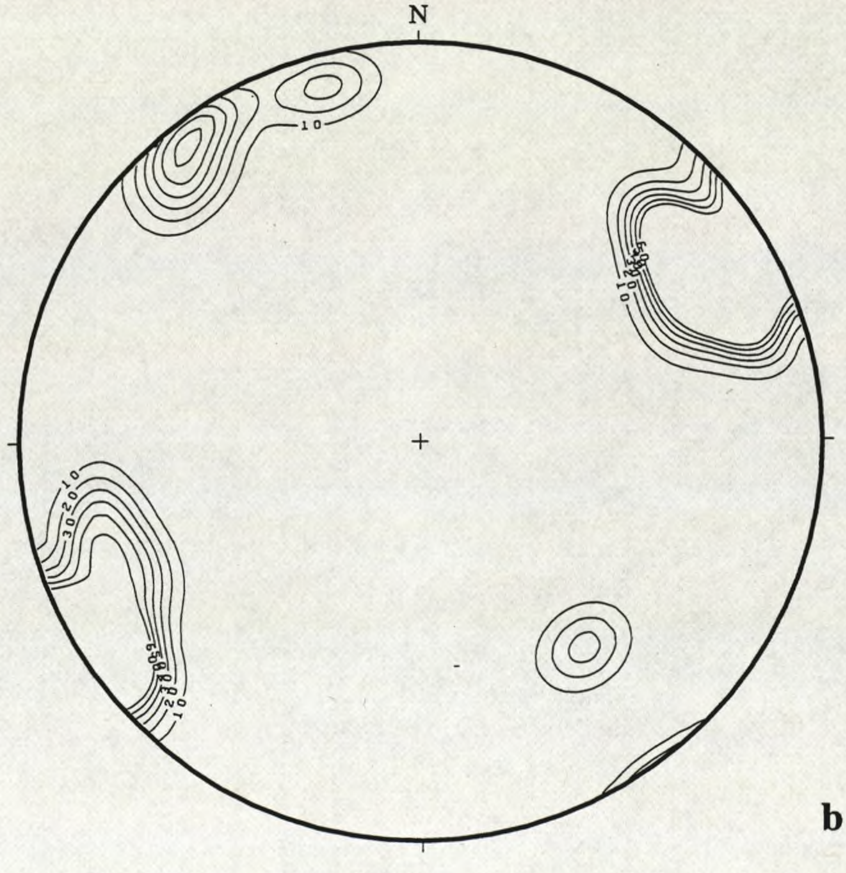

b

Fig. 14

RØRDAL-RD4

Wulff projection

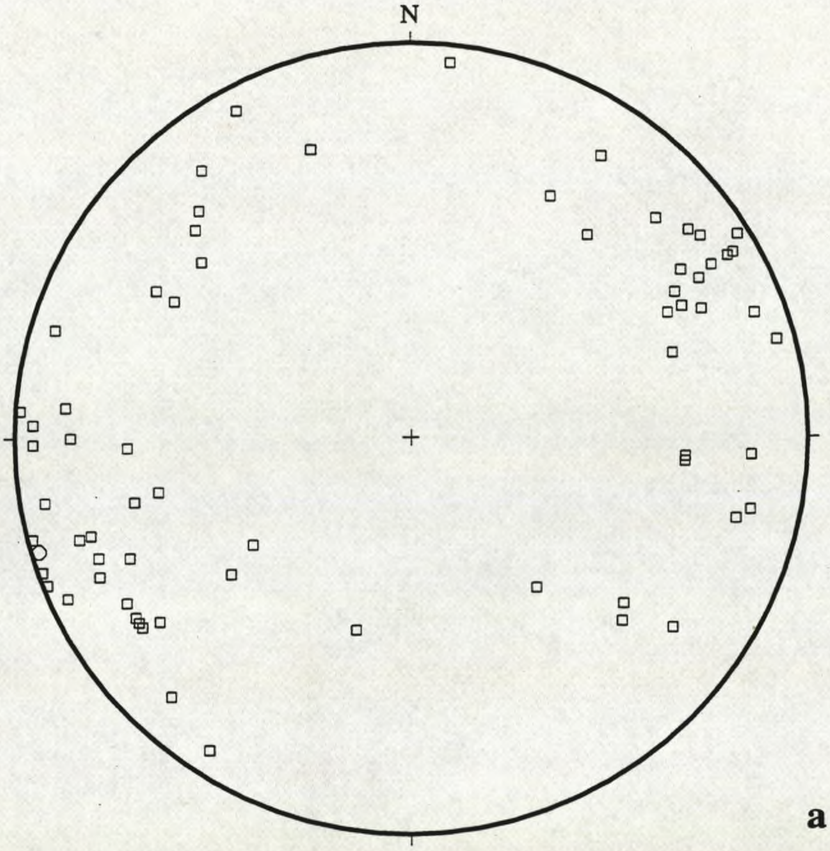

a

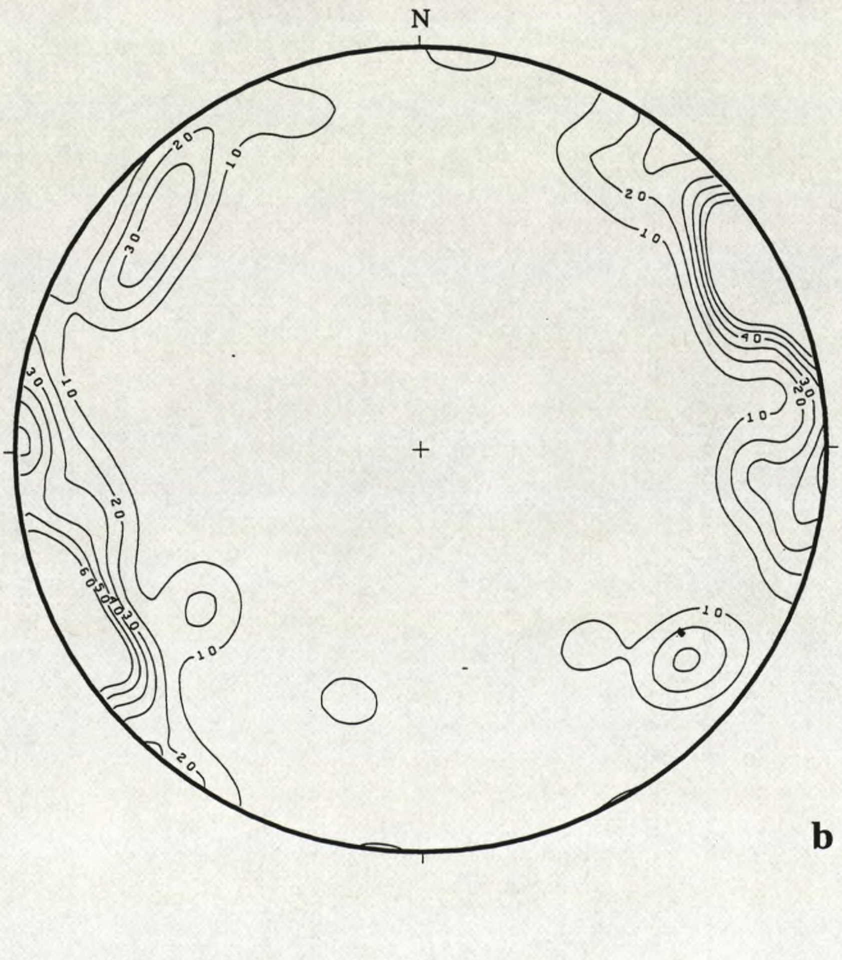

b

Fig. 15

RØRDAL-RD5

Wulff projection

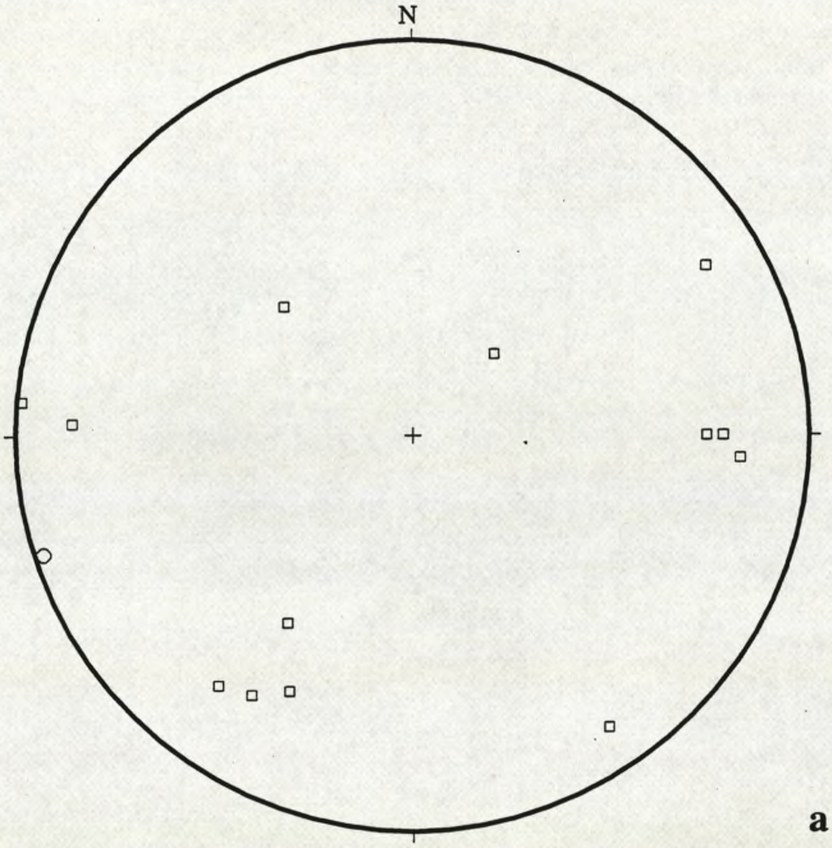

a

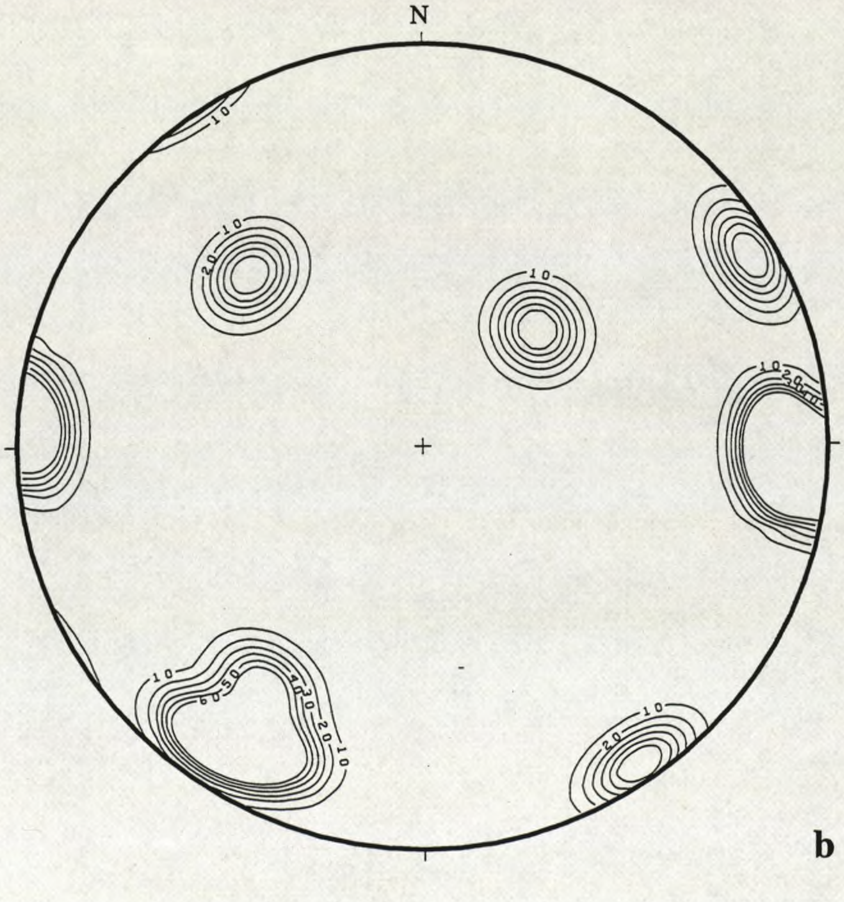

b

Fig. 16

RØRDAL, RD1,RD2,RD3,RD4,RD5

Wulff projection

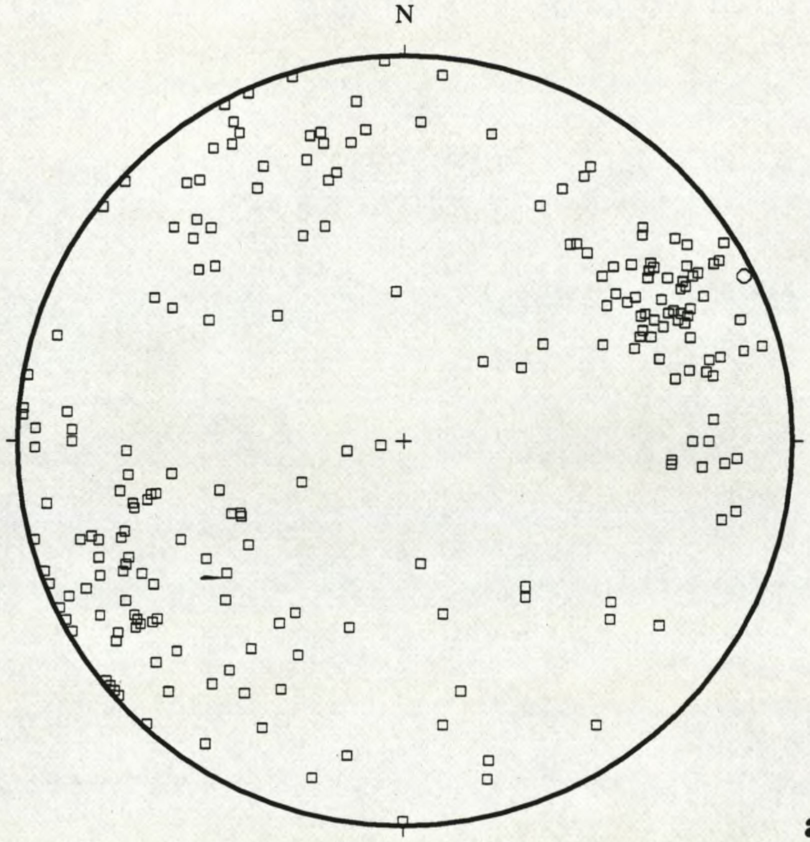

a

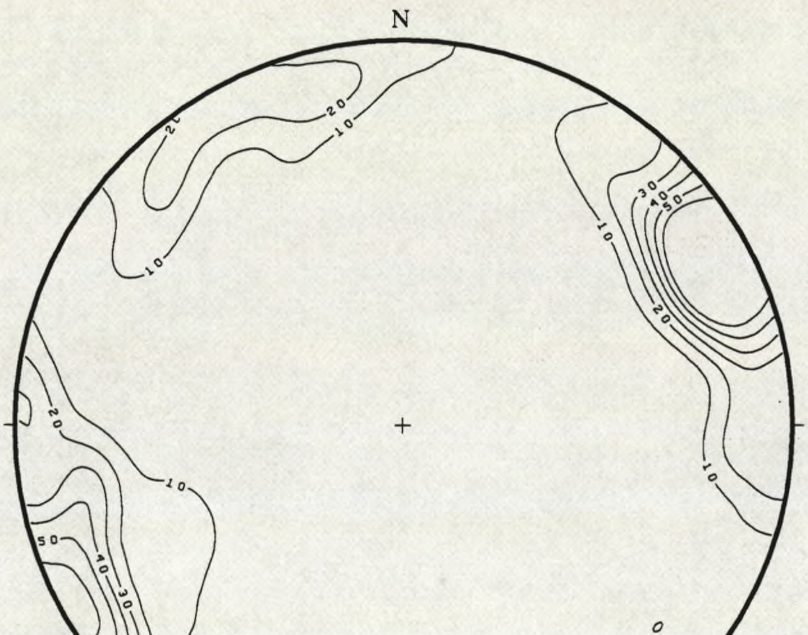

b

Fig. 17

Rørdal strike

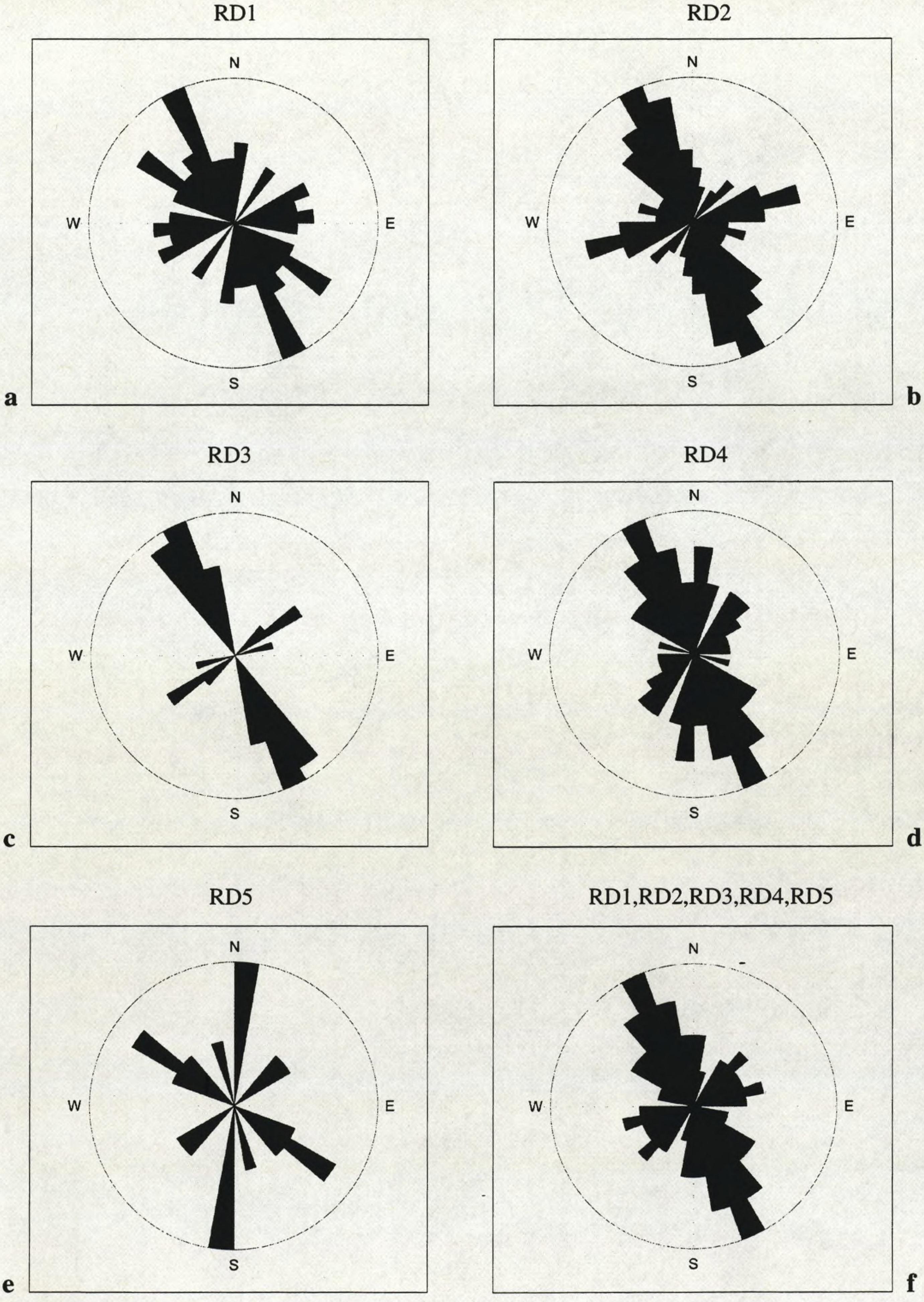

Fig. 18

Rørdal dipdirection

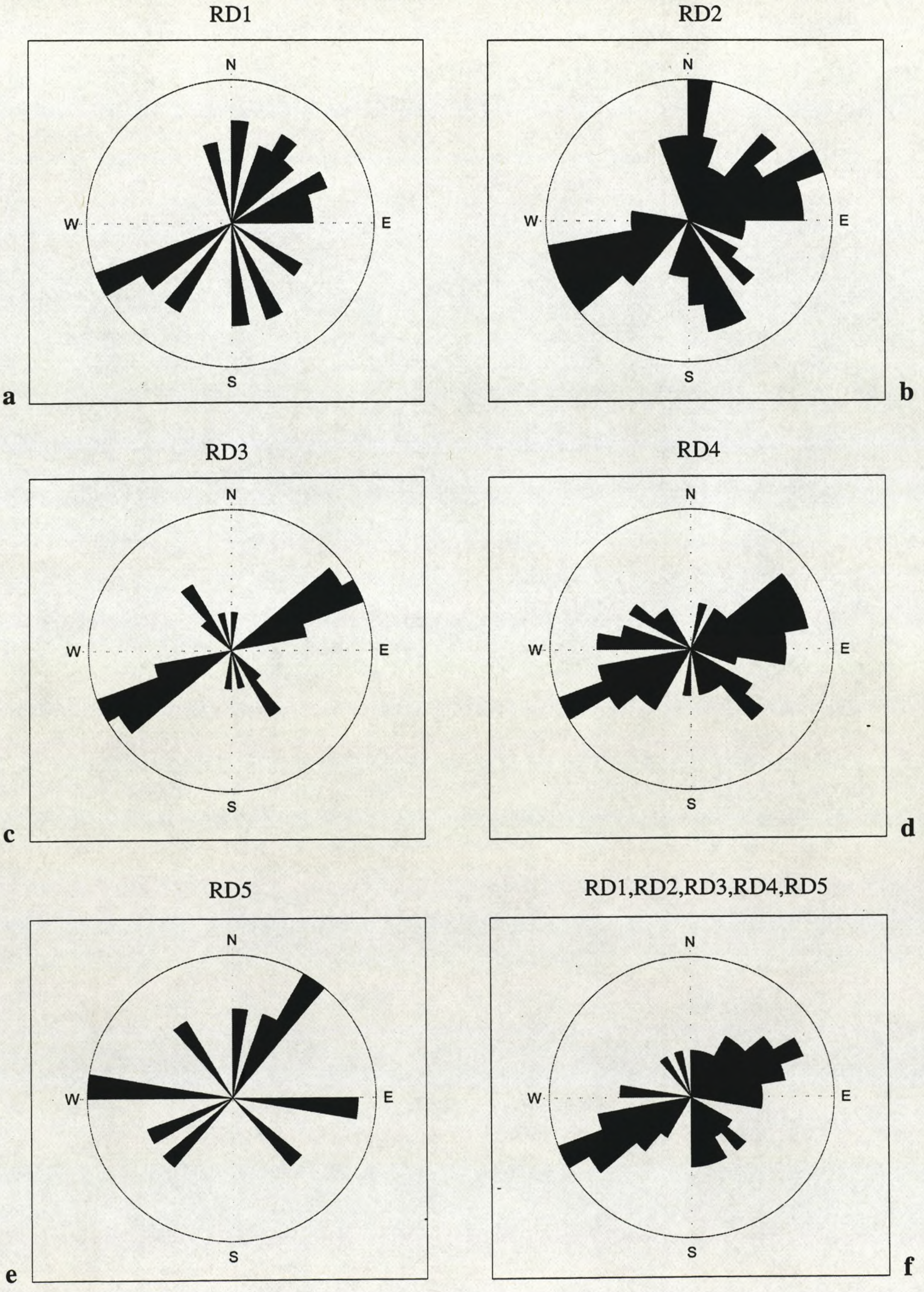

Fig. 19

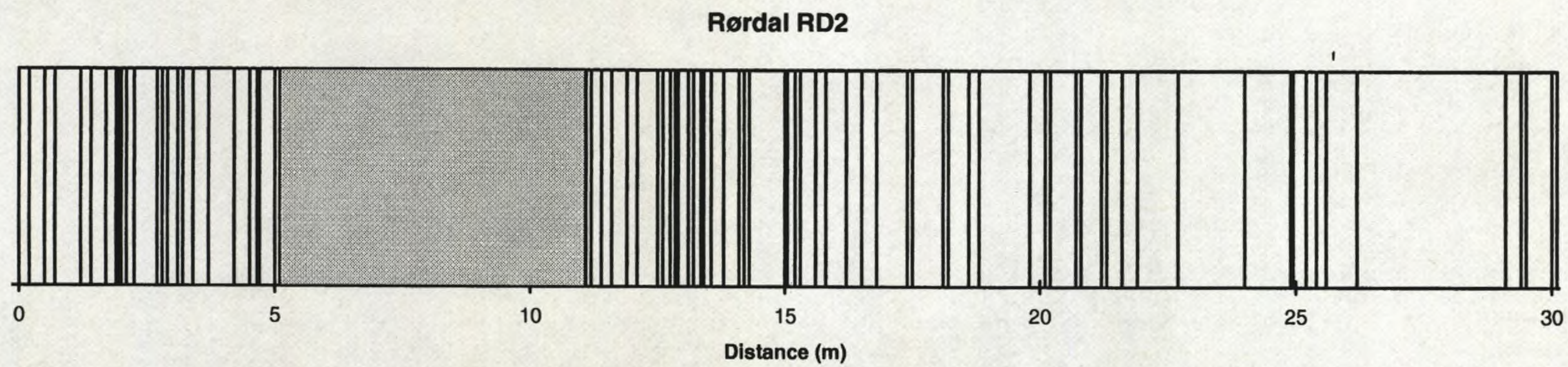

Fig. 20

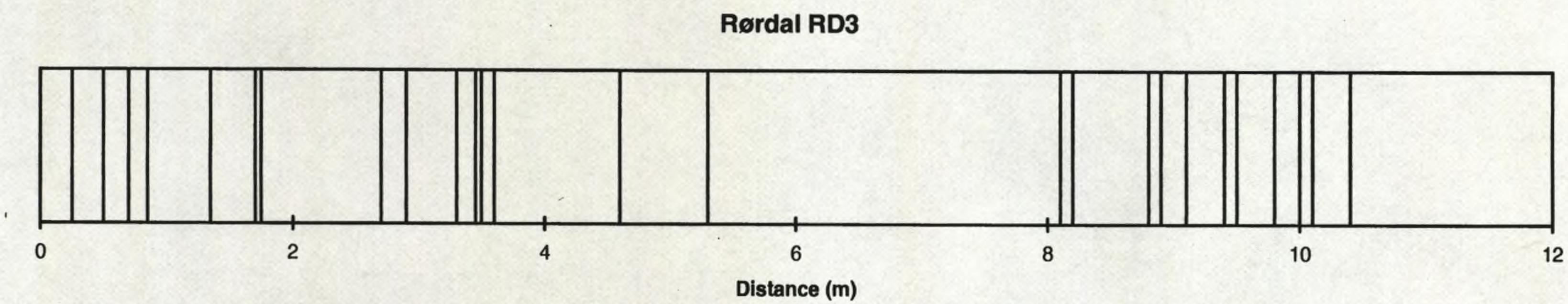

Fig. 21

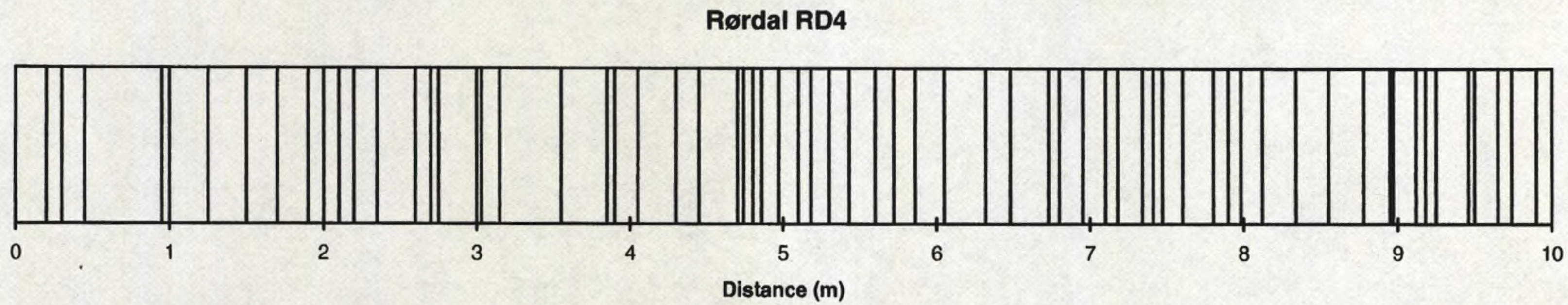

Fig. 22

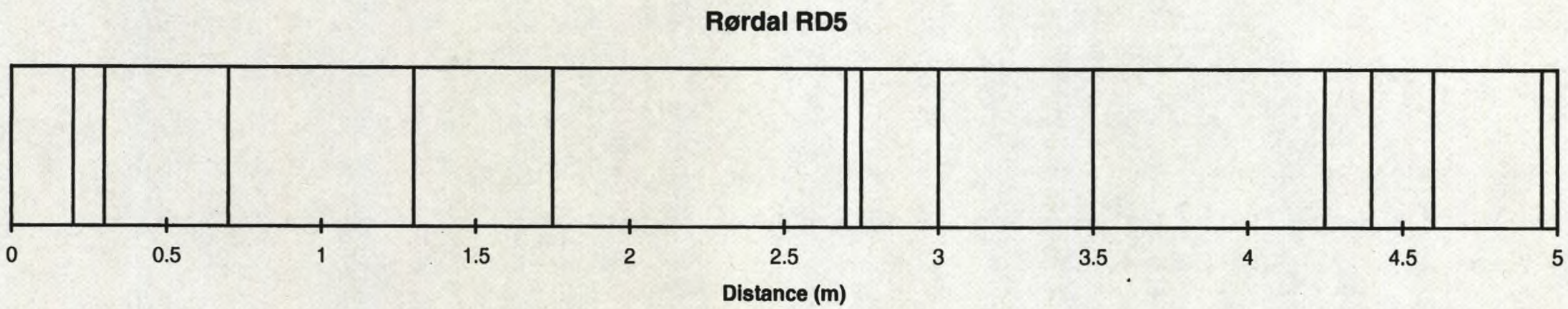

Fig. 23

Rørdal RD2

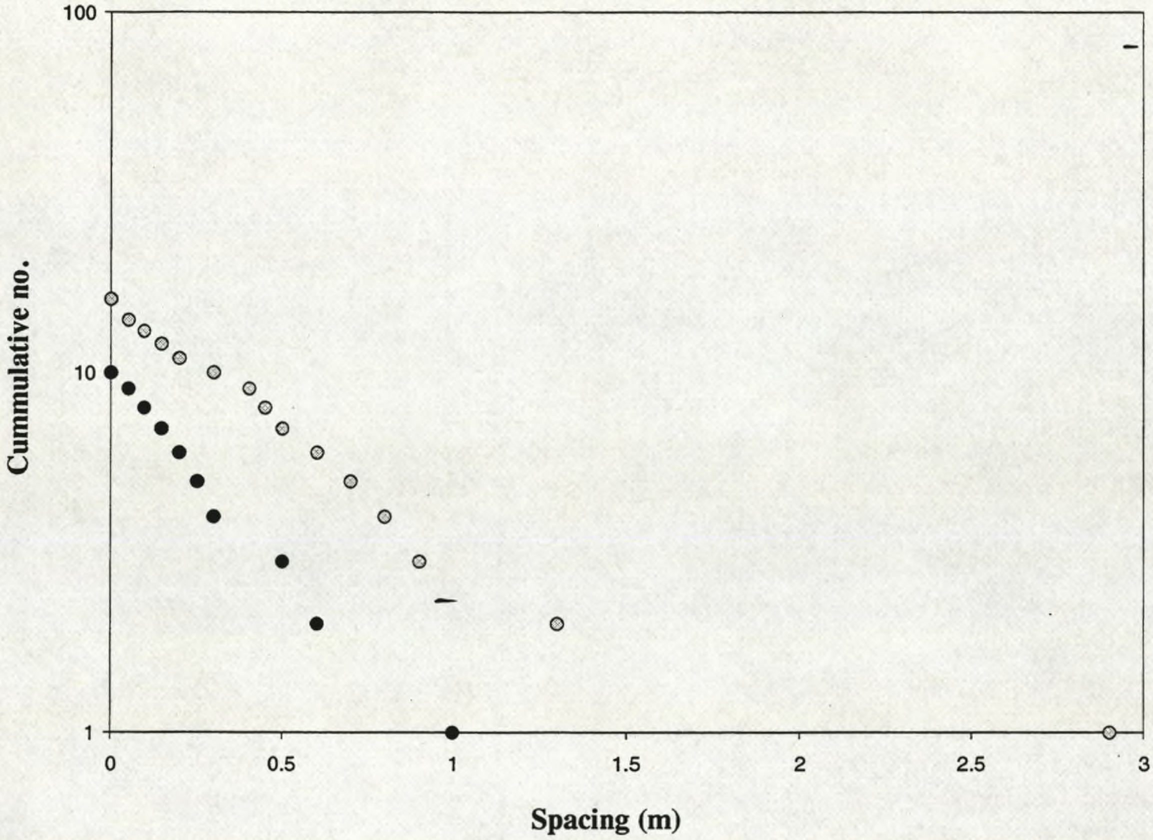

a

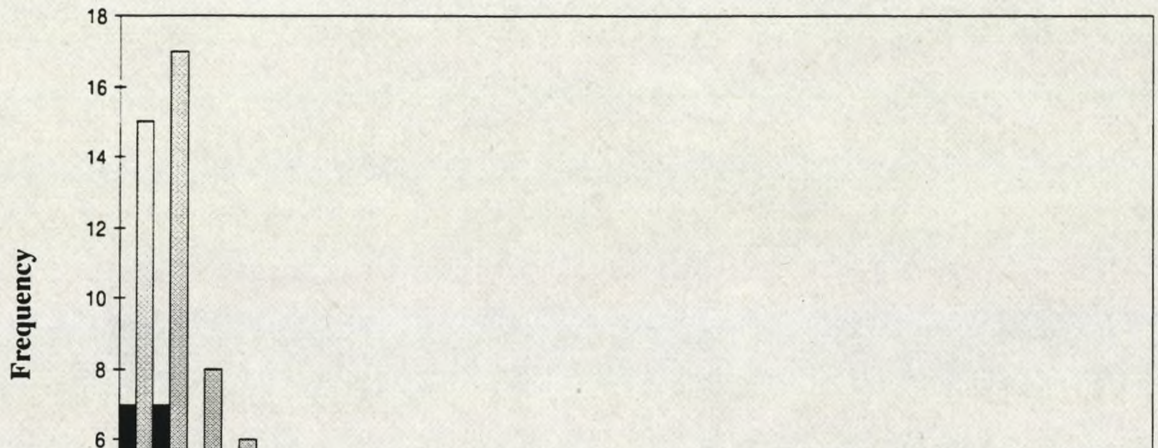

b

Fig. 24

Rørdal RD3

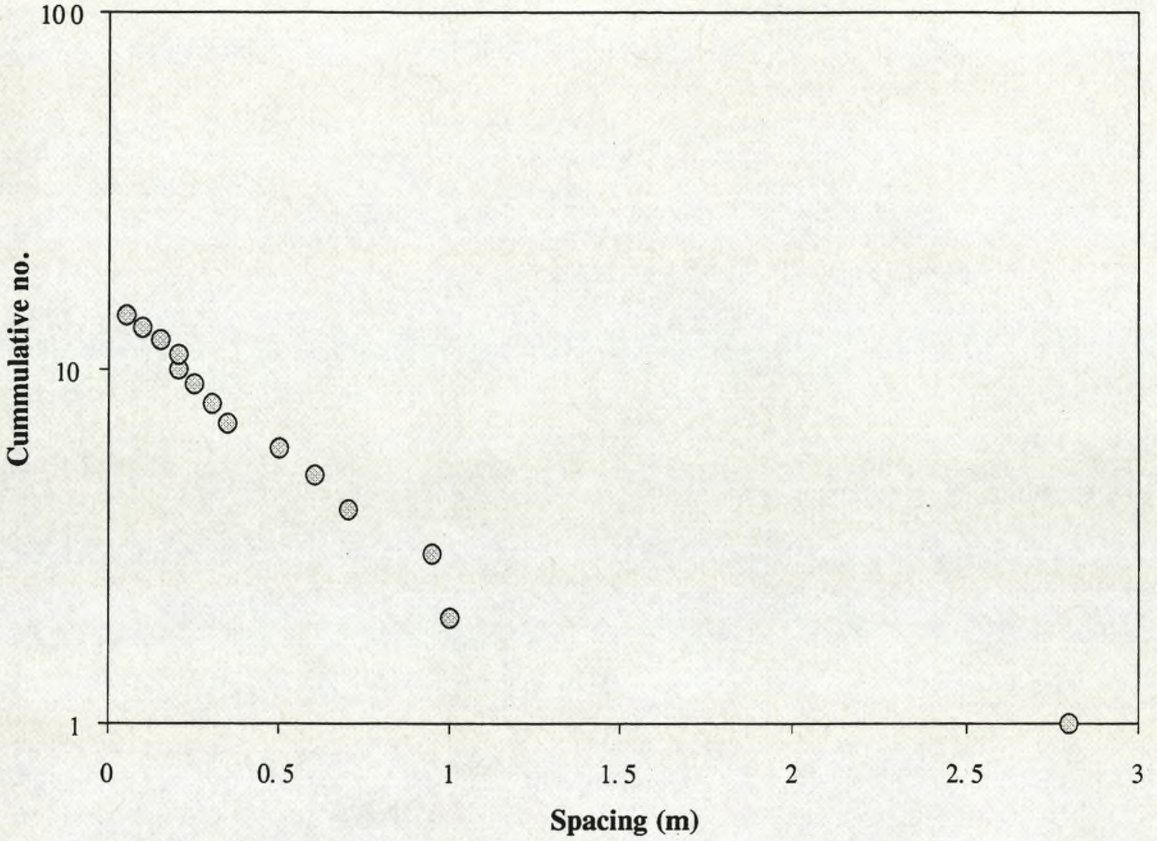

a

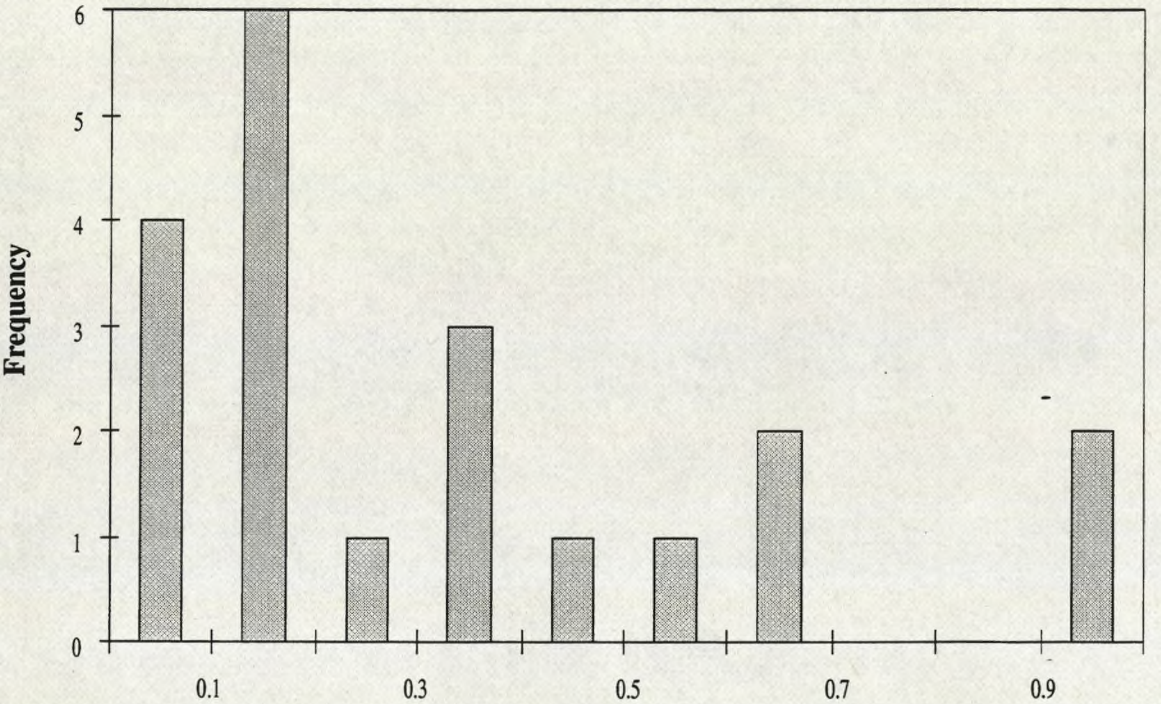

b

Fig. 25

Rørdal RD4

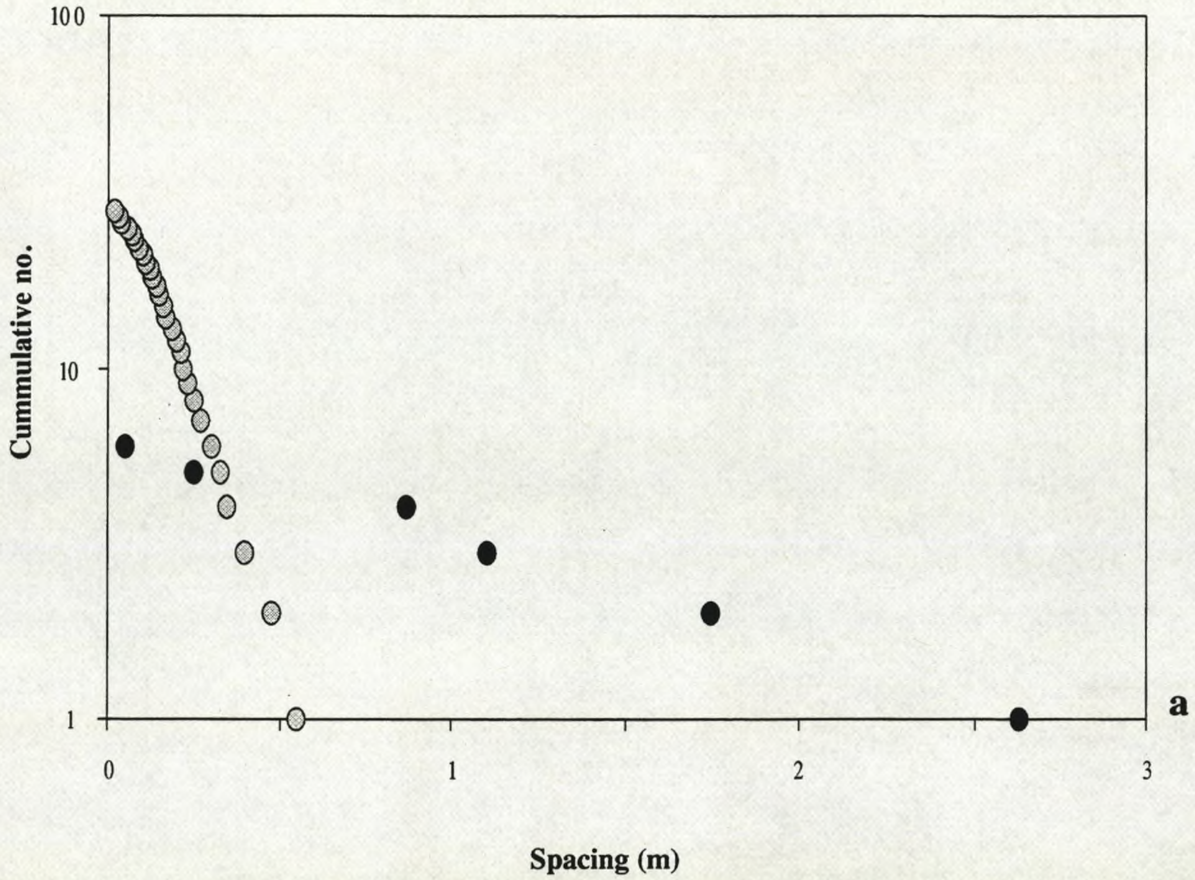

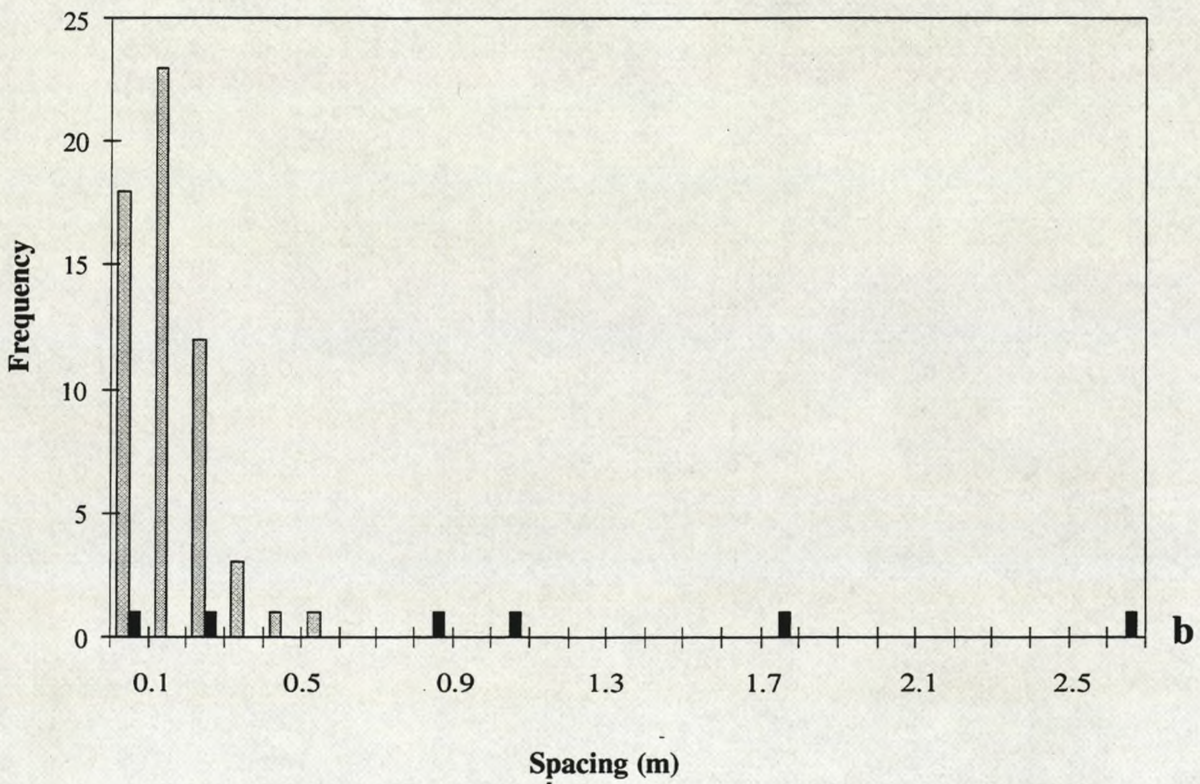

Fig. 26

Rørdal RD5

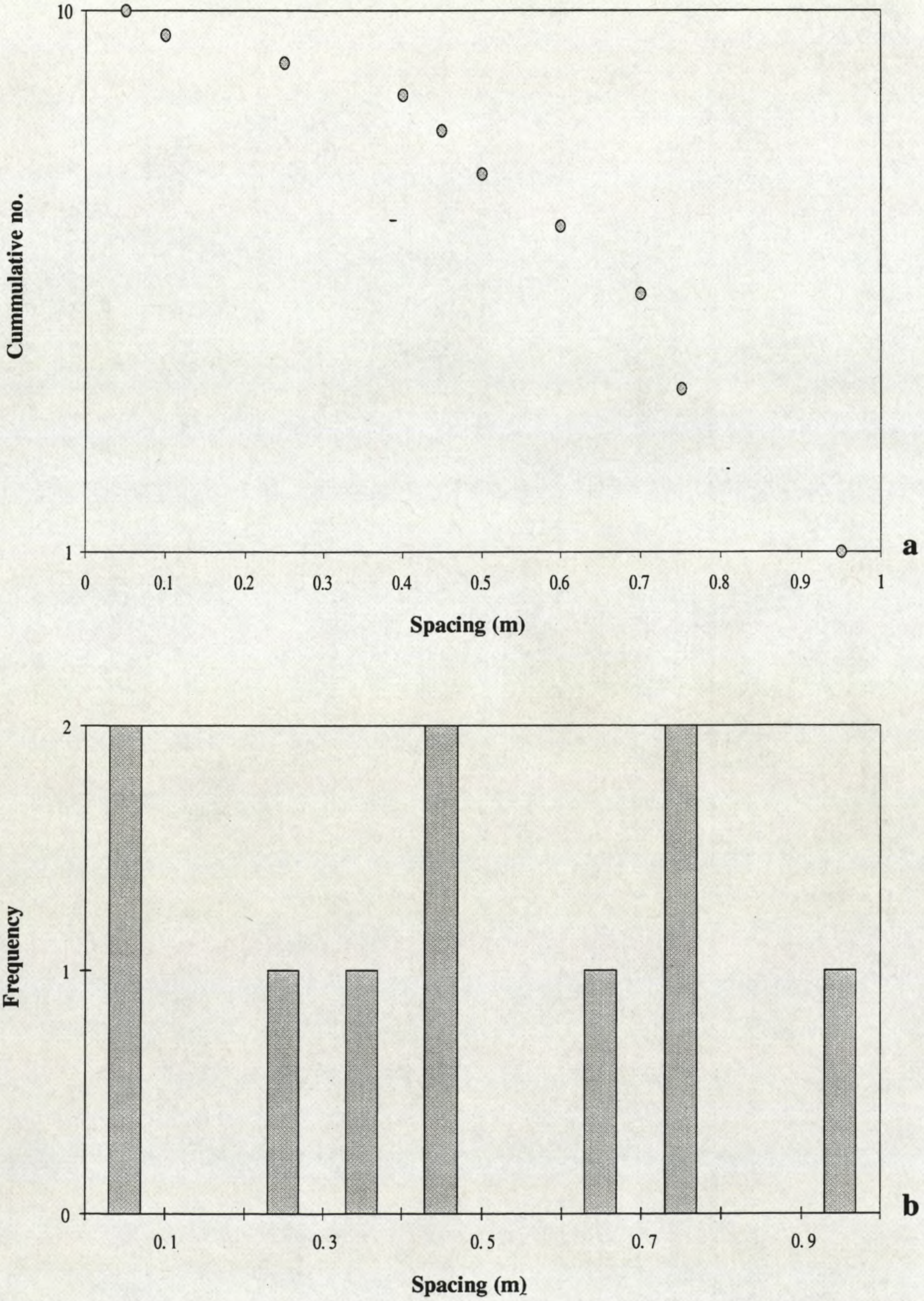

Fig. 27

Rørdal A

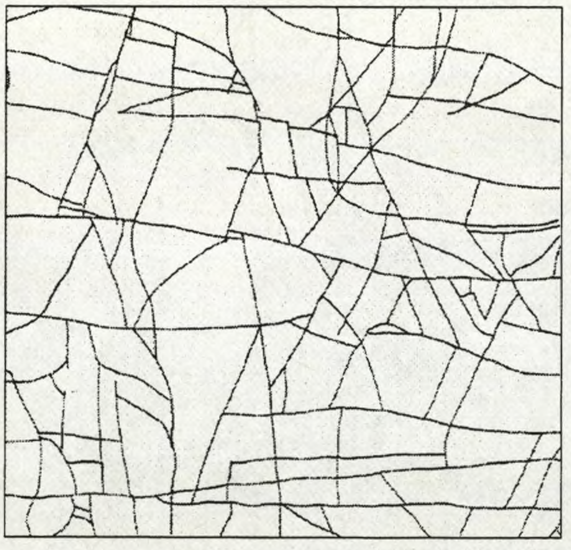

Rørdal B

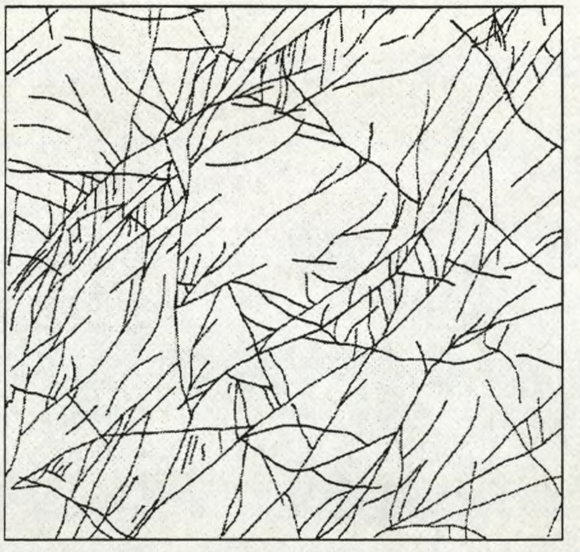

Rørdal C

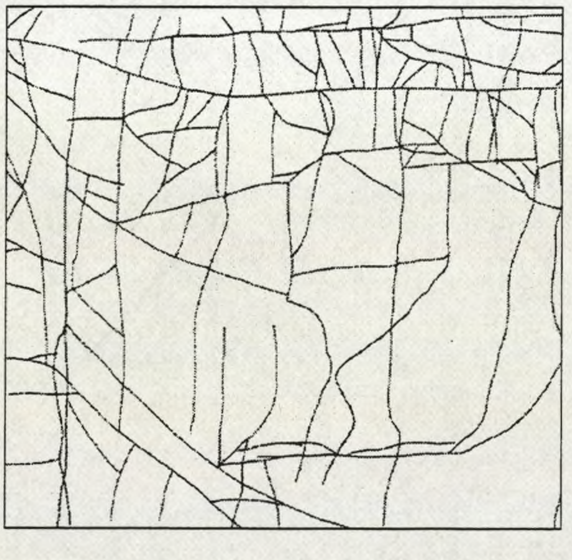

Fig. 28

Rørdal A

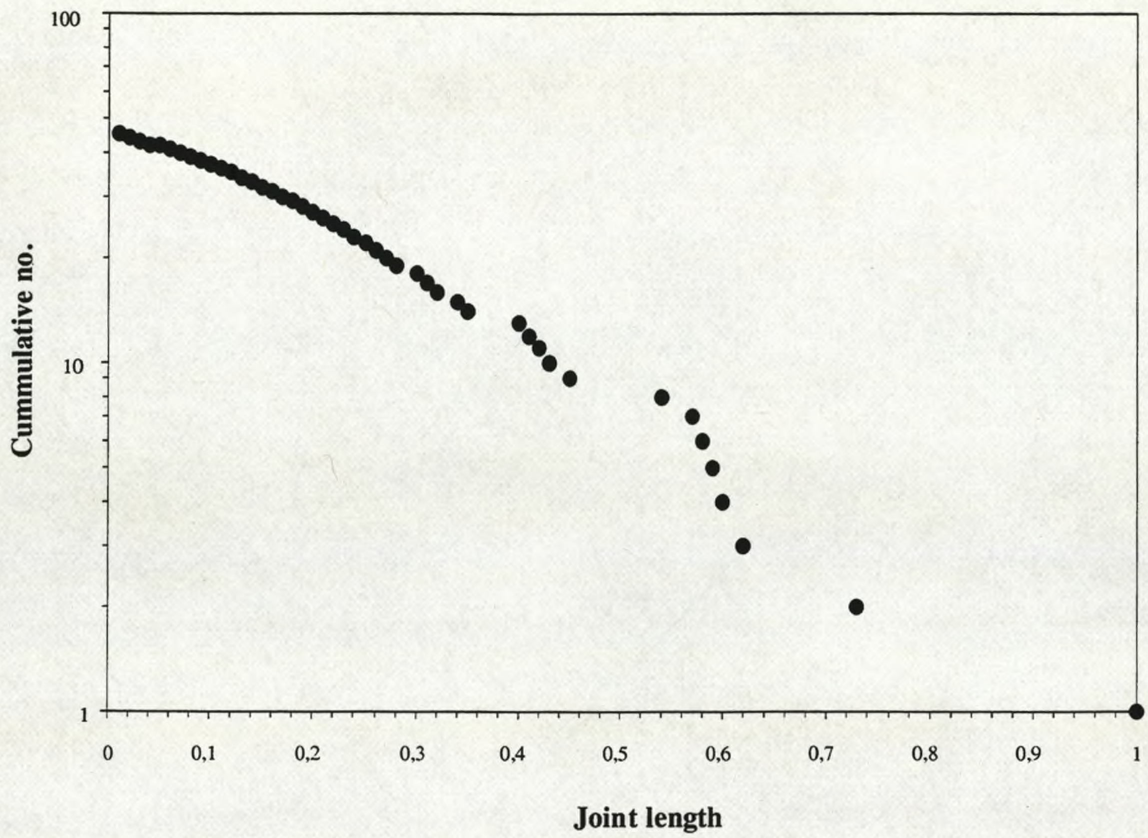

a

b

Fig. 29

Rørdal B

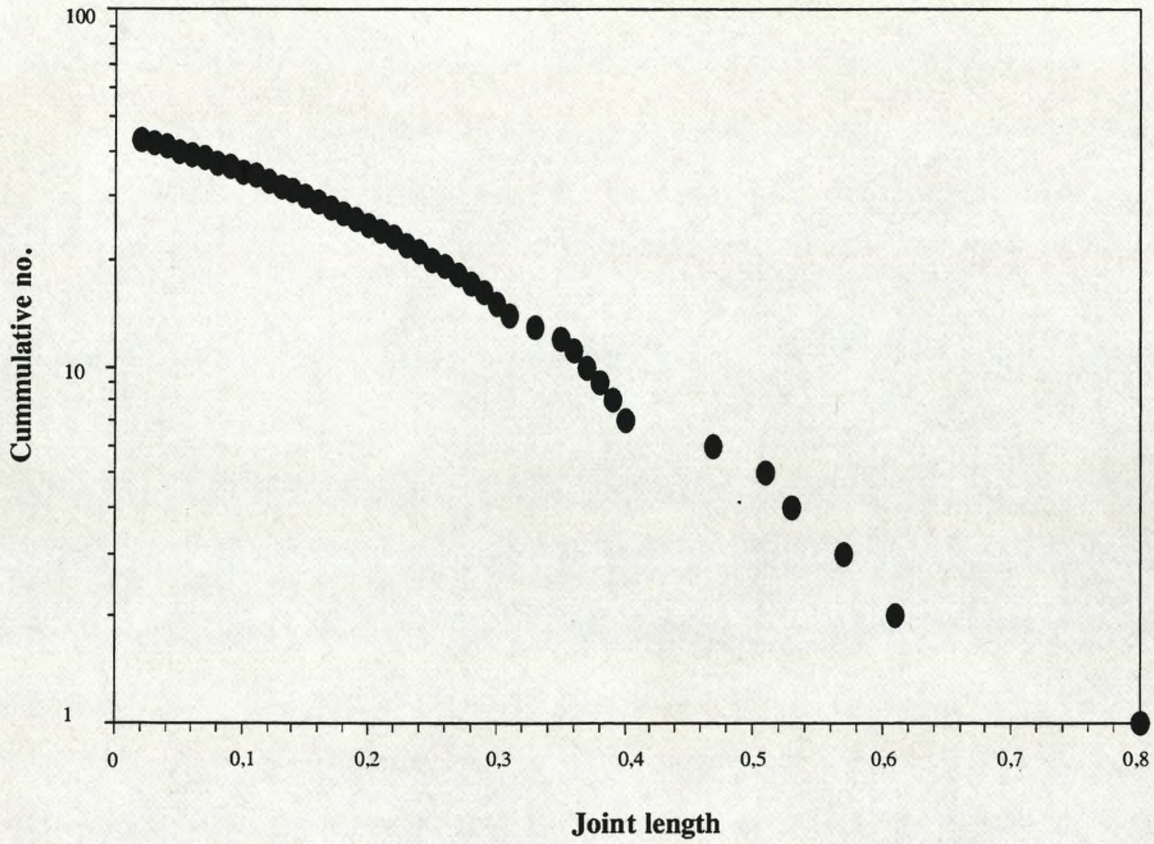

a

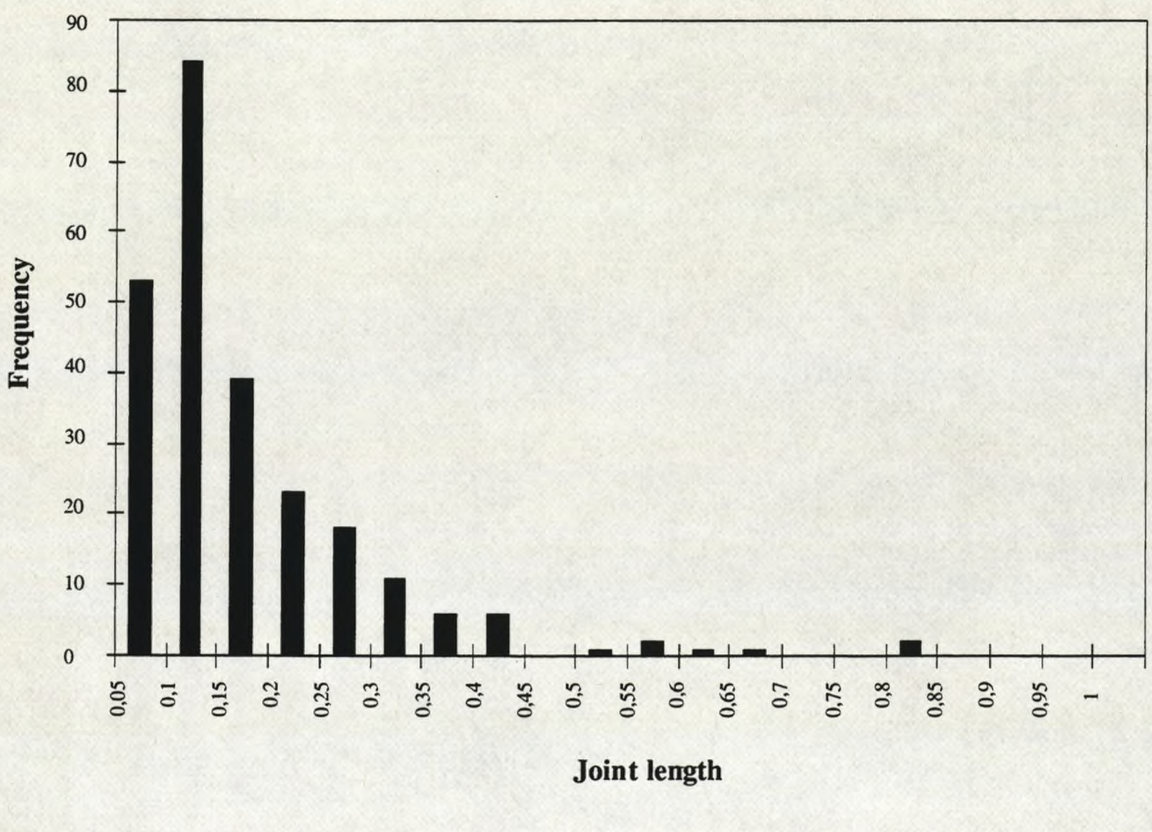

b

Fig. 30

Rørdal C

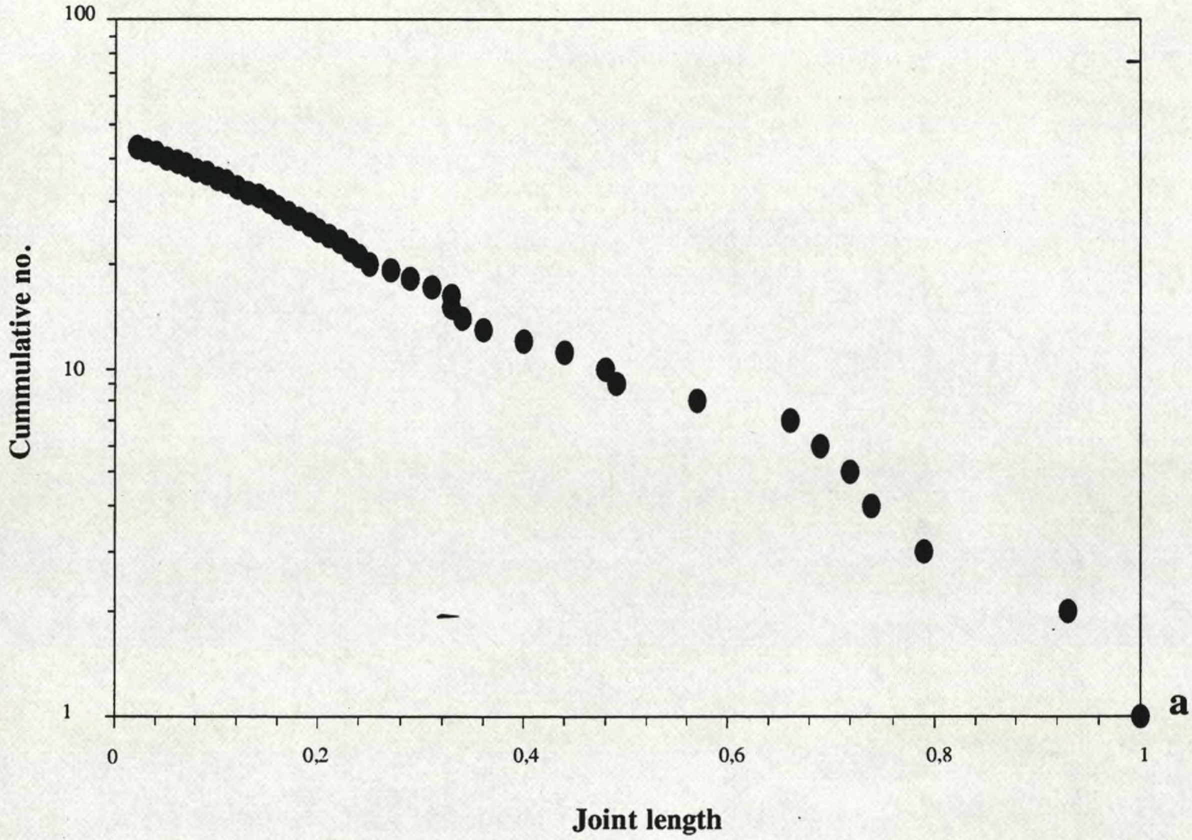

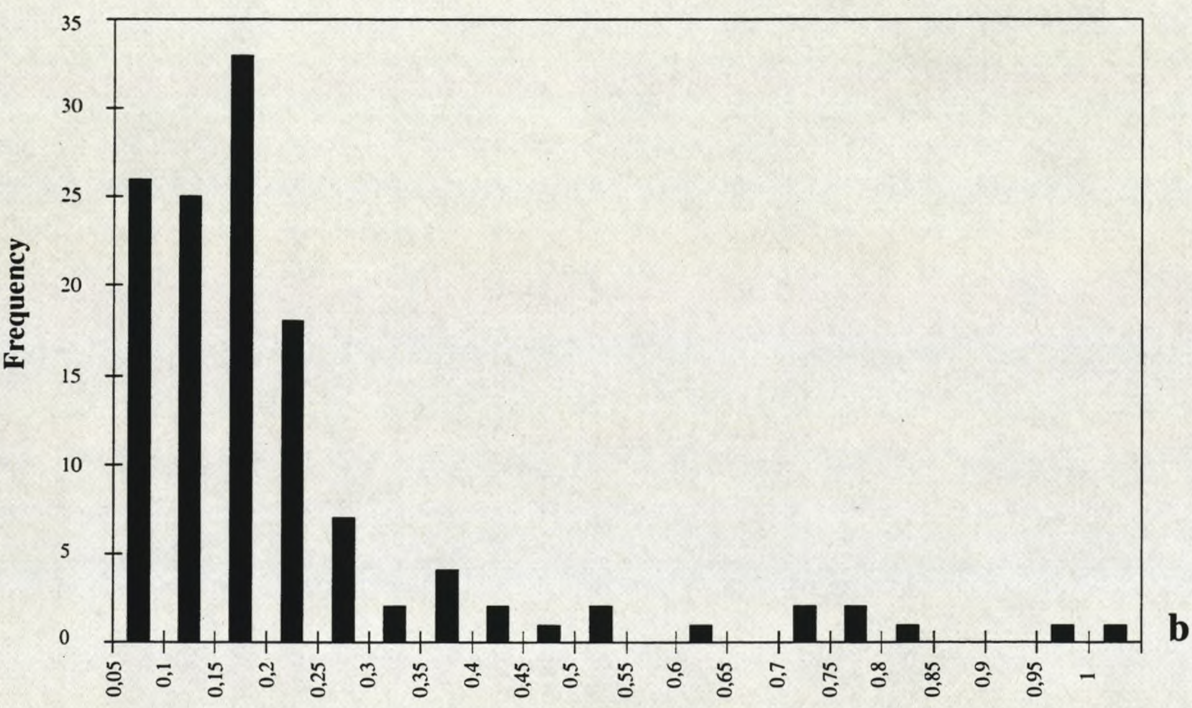

Fig. 31

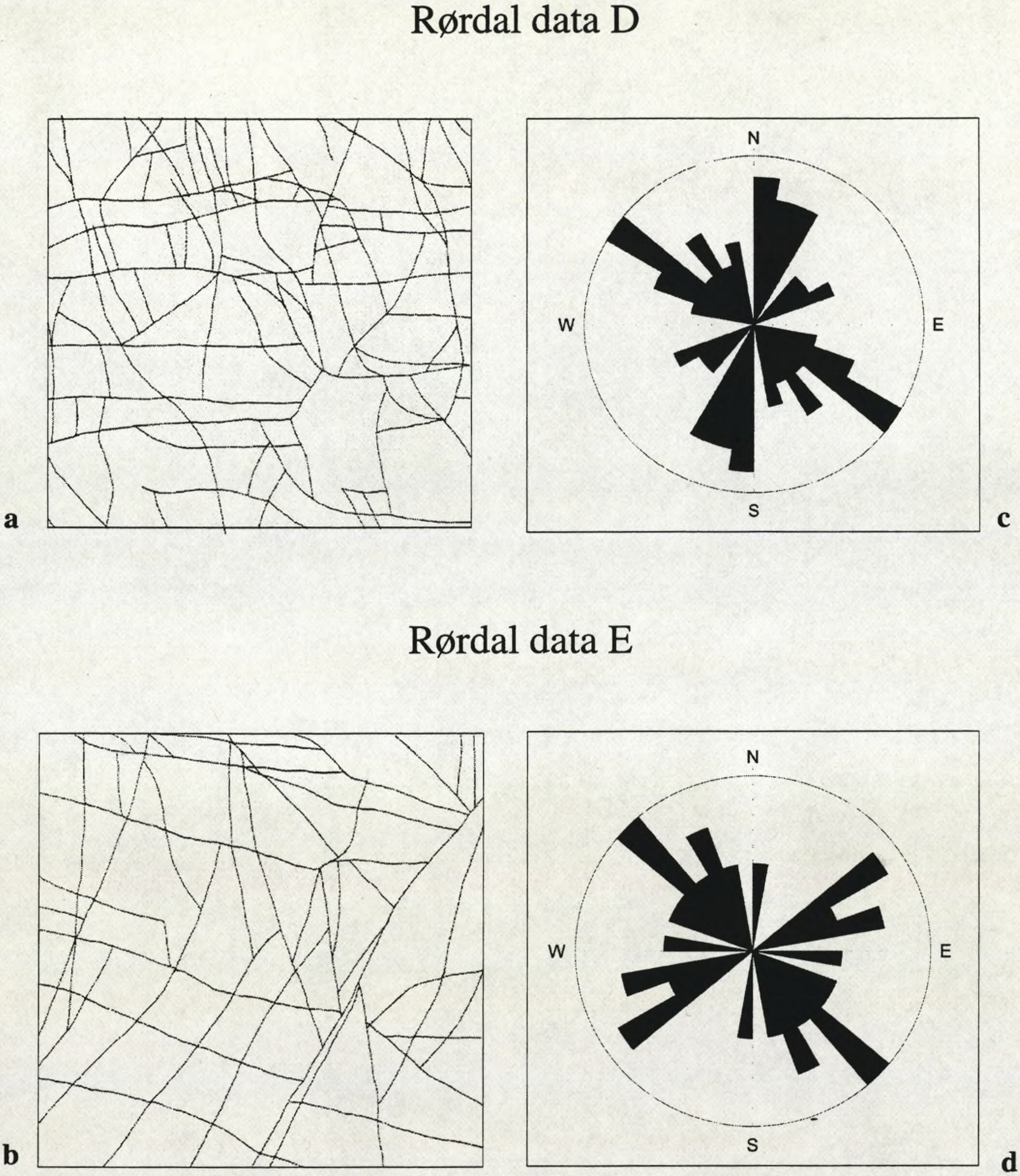

Fig. 32

RØRDAL-RDD

Wulff projection

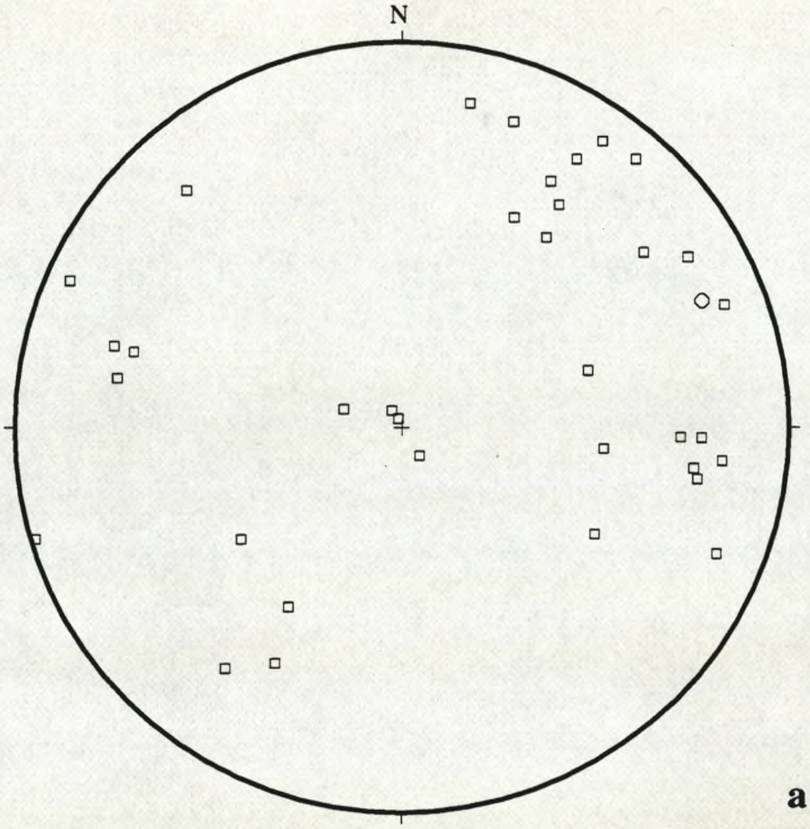

a

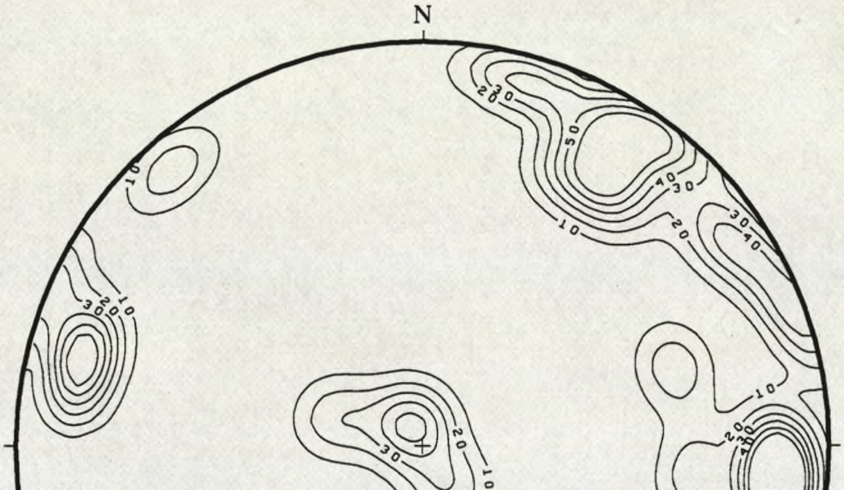

b

Fig. 33

RØRDAL-RDE

Wulff projection

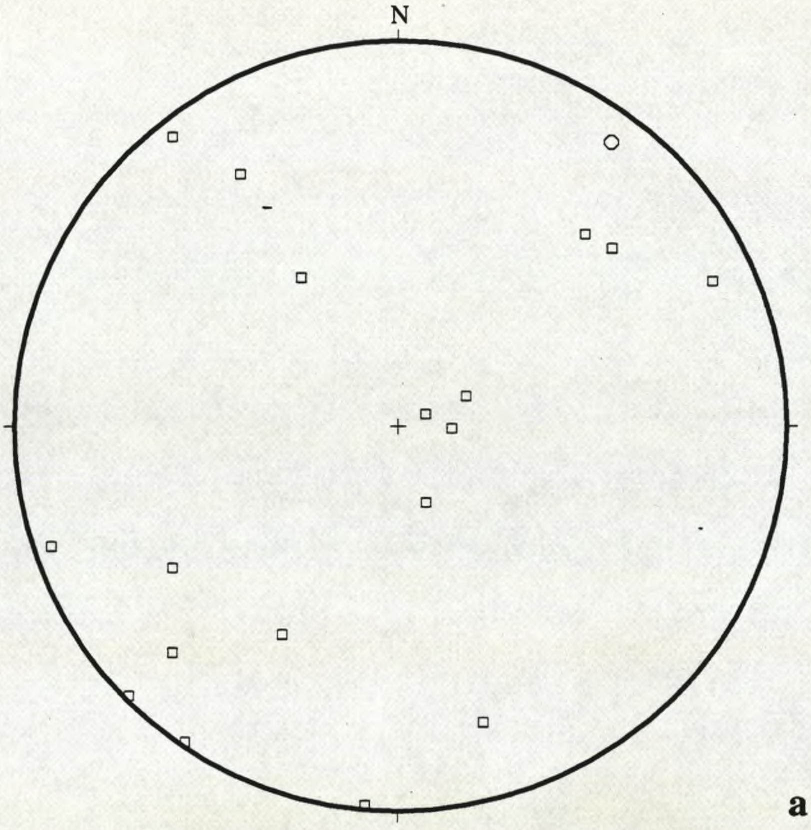

a

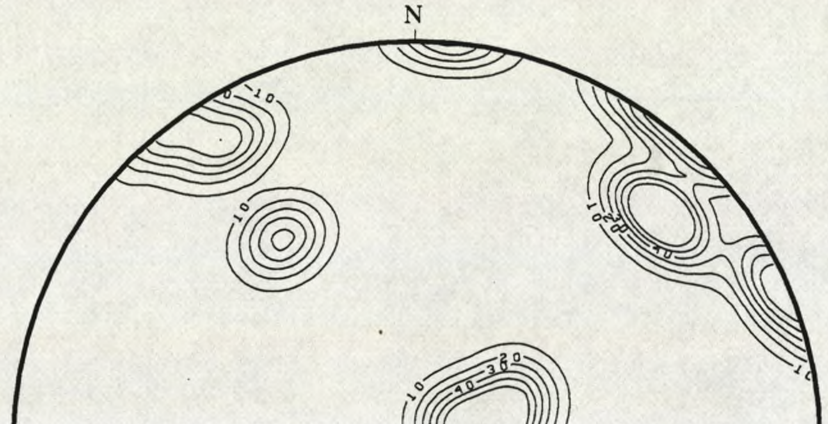

b

Fig. 34

Rørdal dipdirection

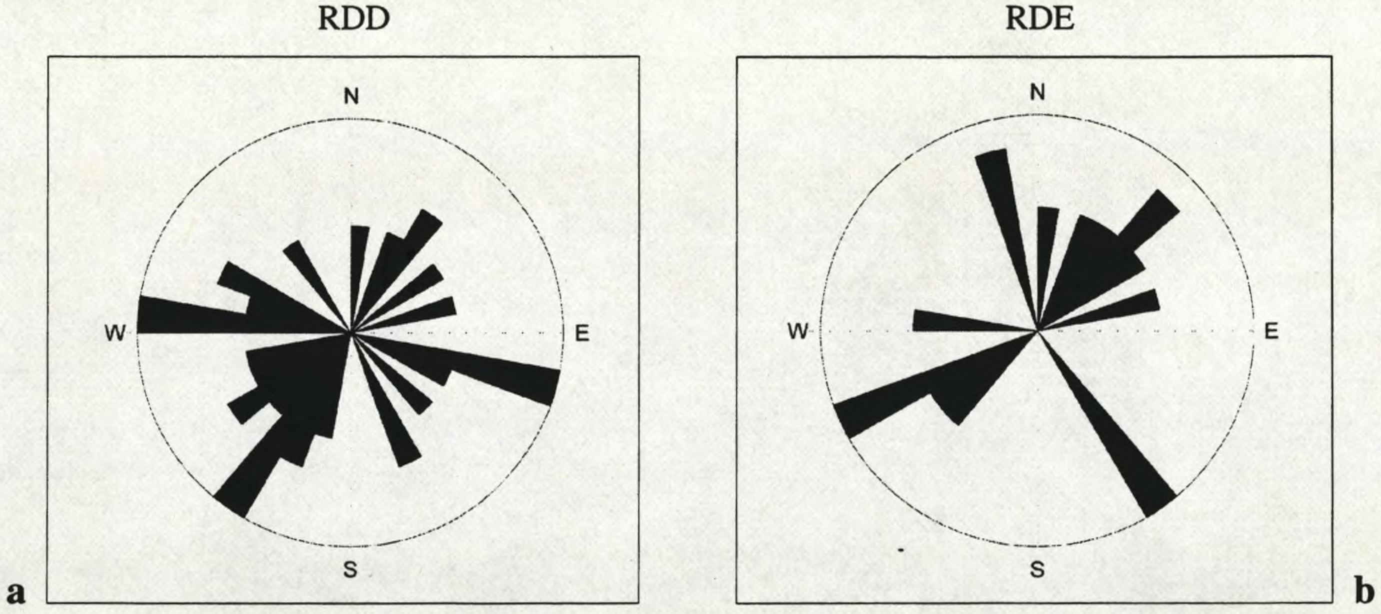

Fig. 35

Rørdal D

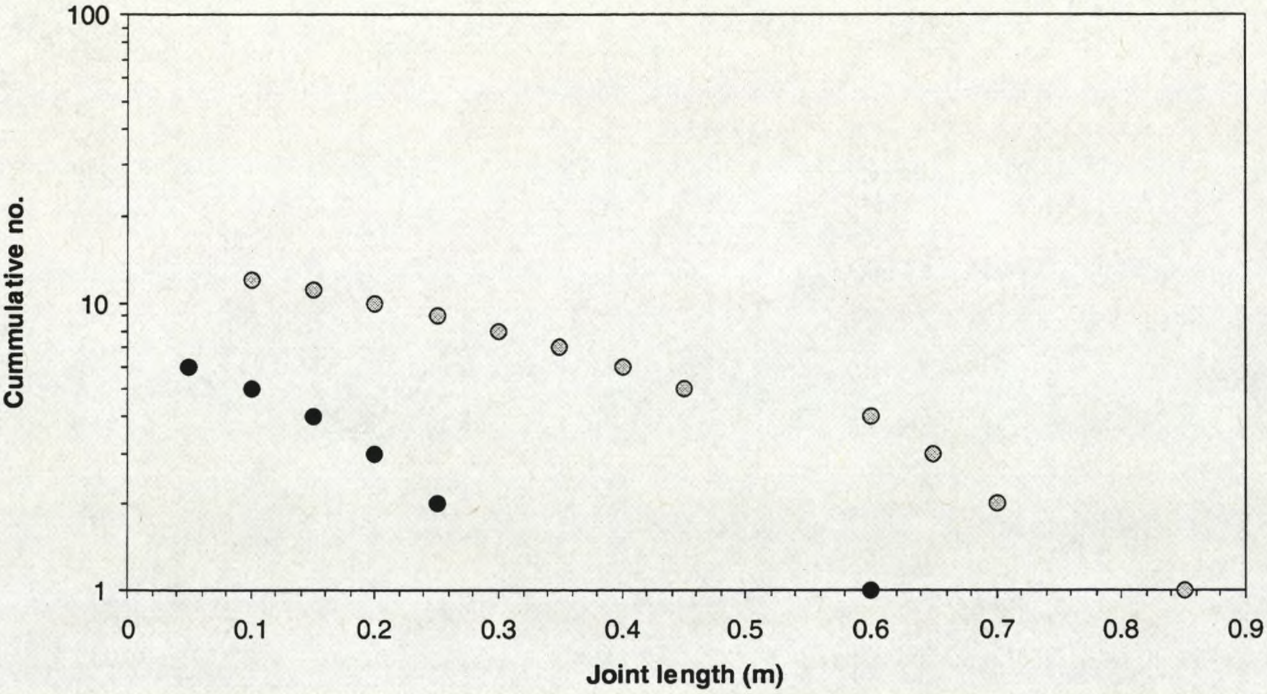

a

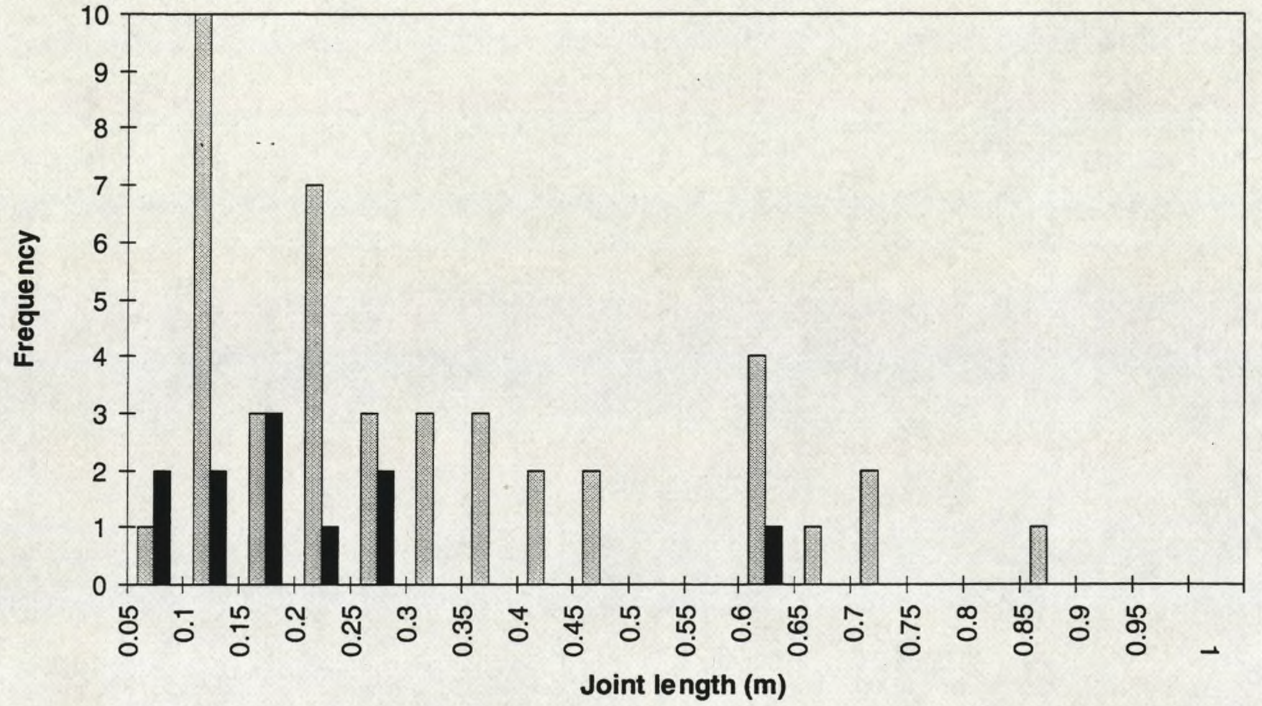

b

Fig. 36

Rørdal E

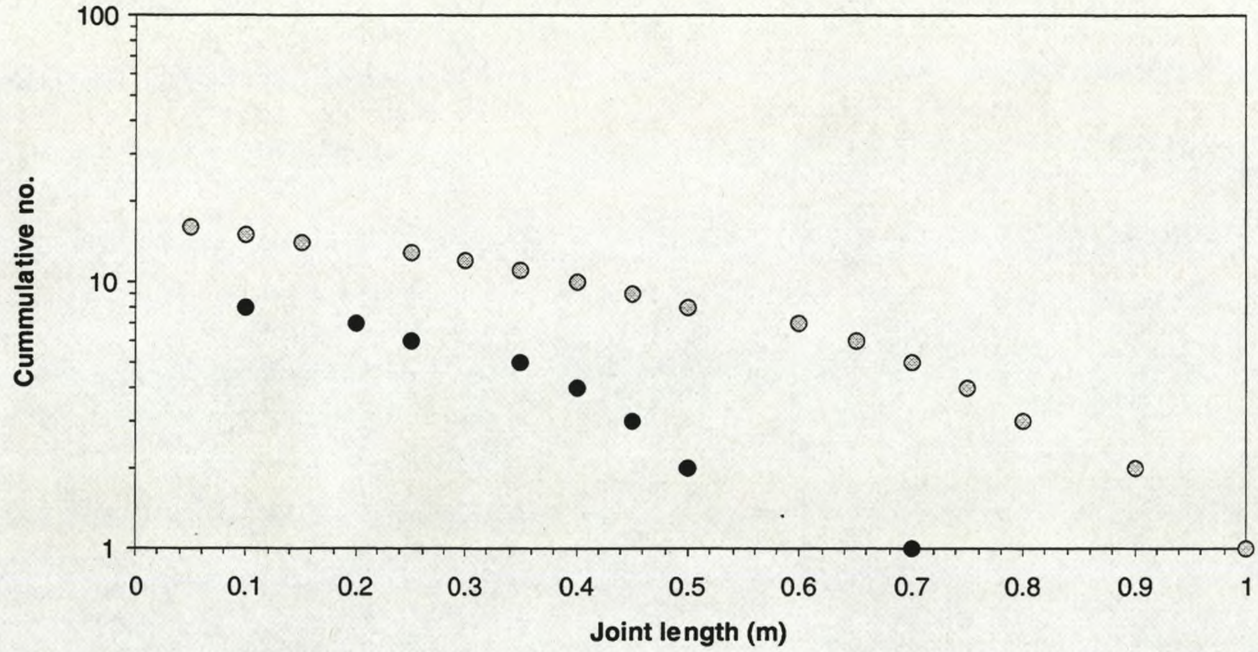

a

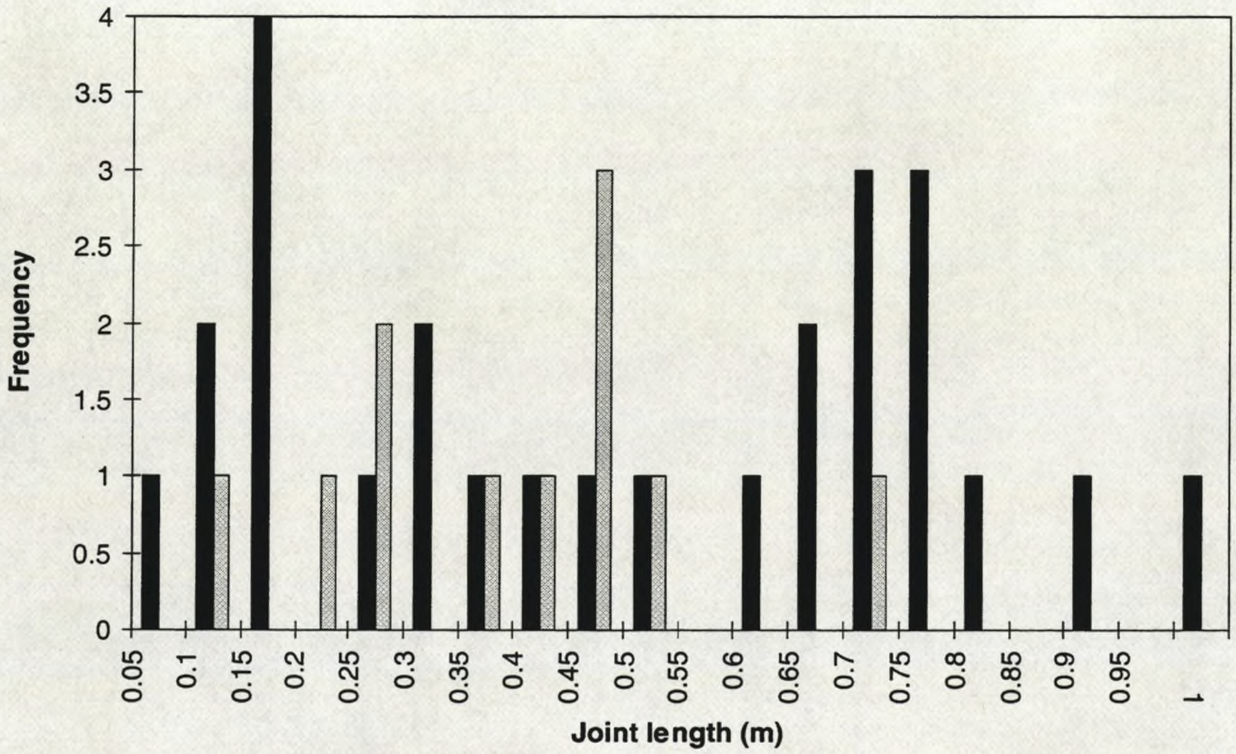

b

Fig. 37